To the root of vegetation-water interactions
Improving spatiotemporal variations in global models

van Oorschot, F.

DOI
10.4233/uuid:674d2760-ca1e-4af8-9afc-ebb18137f05c

Publication date
2024

Document Version
Final published version

Citation (APA)
van Oorschot, F. (2024). *To the root of vegetation-water interactions: Improving spatiotemporal variations in global models*. [Dissertation (TU Delft), Delft University of Technology]. https://doi.org/10.4233/uuid:674d2760-ca1e-4af8-9afc-ebb18137f05c

Supporting information for:

To the root of vegetation-water interactions

Improving spatiotemporal variations in global models

Fransje van Oorschot

October 2024

Contents

List of Figures

List of Tables

Supporting information for chapter 2: Interannual aboveground vegetation variability in the HTESSEL land surface model

S2.1 Model experiments

Table S2.1: Details of offline model experiments

	Spin-up 1993-1999			Evaluation 1999-2019		
Experiment	**LC**	**LAI**	**FCover**	**LC**	**LAI**	**FCover**
CTR	ESA-CCI 1993	CGLS climatology 1993-2019	k=0.5	ESA-CCI 1993	CGLS climatology 1993-2019	k=0.5
IALC	ESA-CCI annually varying 1993-2019	CGLS climatology 1993-2019	k=0.5	ESA-CCI annually varying 1993-2019	CGLS climatology 1993-2019	k=0.5
IAK5	ESA-CCI annually varying 1993-2019	CGLS inter-annually varying 1993-2019	k=0.5	ESA-CCI annually varying 1993-2019	CGLS inter-annually varying 1993-2019	k=0.5
IAKV	ESA-CCI annually varying 1993-2019	CGLS inter-annually varying 1993-2019	k vegetation specific	ESA-CCI annually varying 1993-2019	CGLS inter-annually varying 1993-2019	k vegetation specific

S2.2 Land cover results

Table S2.2: Annual mean (2014-2018) evaporation fluxes (mm/year) with E total evaporation, E_t transpiration, E_s soil evaporation and E_i interception evaporation in experiments CTR and IALC and DOLCEv3 (only E) for the three cases highlighted in Fig. 2.3

Case	E **CTR**	E **IALC**	E **DOLCEv3**	E_t **CTR**	E_t **IALC**	E_s **CTR**	E_s **IALC**	E_i **CTR**	E_i **IALC**
Amazon	1174	1162	1160	633	615	156	183	384	363
Lapland	202	206	252	43	49	116	112	39	41
Central Asia	279	280	287	29	30	222	220	13	13

Table S2.3: Pearson correlation values (r) and root mean squared error (RMSE) of model monthly evaporation with respect to DOLCEv3 evaporation, and near-surface soil moisture with respect to ESA-CCI SM. For r inter-annual anomalies are used, for RMSE E the monthly values, and for RMSE $\mathrm{SM_s}$ the standardized inter-annual anomalies. The cases are highlighted in Fig. 2.3, S2.1-S2.3

Case	r E **CTR**	r E **IALC**	**RMSE** E **CTR**	**RMSE** E **IALC**	r $\mathrm{SM_s}$ **CTR**	r $\mathrm{SM_s}$ **IALC**	**RMSE** $\mathrm{SM_s}$ **CTR**	**RMSE** $\mathrm{SM_s}$ **IALC**
Amazon	0.64	0.64	0.43	0.44	0.059	0.056	1.01	1.01
Lapland	0.56	0.56	0.28	0.27	0.034	0.034	1.33	1.33
Central Asia	0.76	0.76	0.33	0.33	0.24	0.24	0.81	0.81

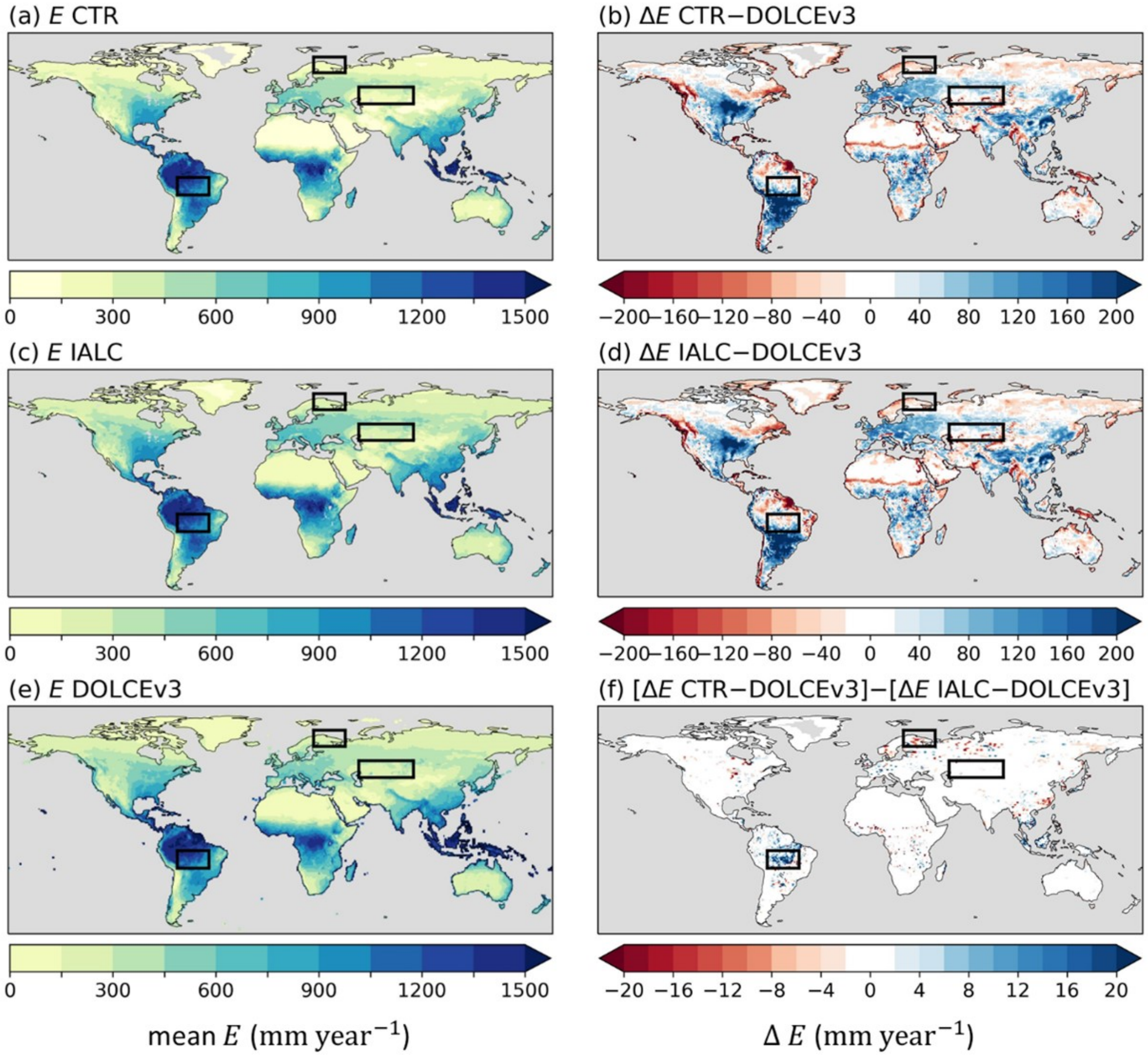

Figure S2.1: Mean evaporation (E) for (a) CTR, (c) IALC and (E) DOLCEv3 for 2014-2018. (b) and (d) show the absolute difference of mean E between CTR and DOLCEv3, and IALC and DOLCEv3. (f) is the difference between (b) and (d).

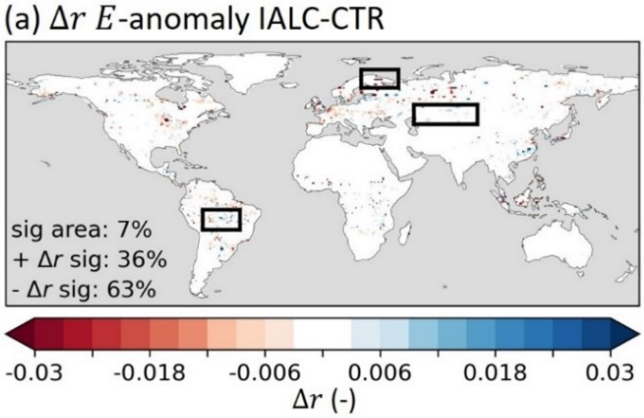

Figure S2.2: Pearson correlation difference between experiment CTR and IALC (IALC-CTR) for (a) monthly anomaly total evaporation (E) with respect to DOLCEv3 evaporation and (b) monthly anomaly surface soil moisture (SM_s) with respect to ESA-CCI SM. Blue (red) indicates an increased (reduced) correlation in IALC compared to CTR, white indicates small and/or insignificant r differences, and grey indicates no data points. The percentages indicate the areal percentage of significantly changing land points, and the areal percentage of positive and negative Δr for significant points. The boxes highlight the three regions Southern Amazon, Lapland and Central Asia with major land cover changes. See Table S2.1 for details of the experiments and Table S2.2 for values in the highlighted regions.

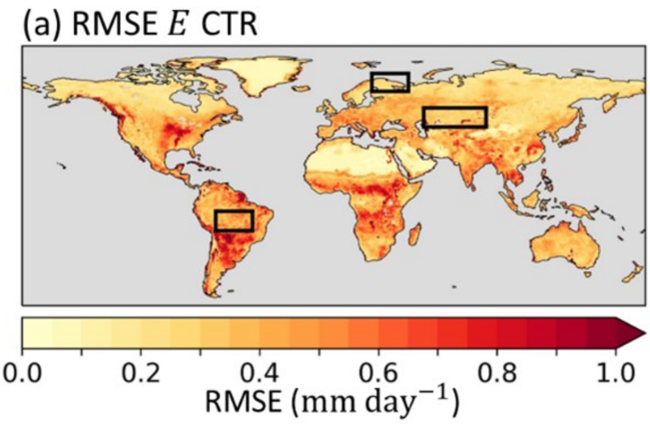

Figure S2.3: (a) Root mean squared error (RMSE) of model monthly evaporation in experiment CTR with respect to DOLCEv3 with red indicating a larger RMSE. (b) The difference between RMSE in CTR and IALC (IALC–CTR) with blue (red) indicating a reduced (increased) RMSE. The boxes highlight the three regions Southern Amazon, Lapland and Central Asia with major land cover changes. See Table S2.1 for details of the experiments and Table S2.2 for values in the highlighted regions.

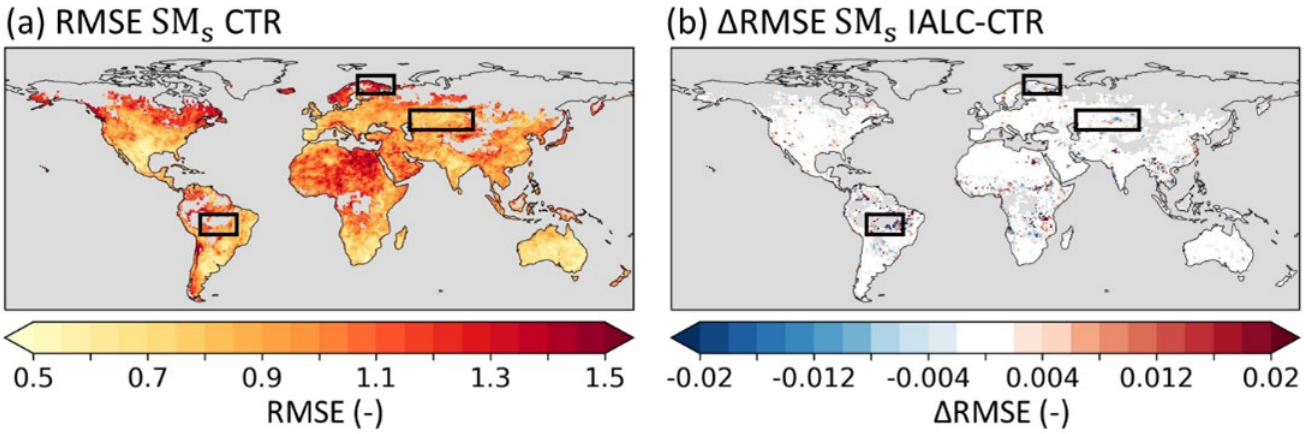

Figure S2.4: (a) Root mean squared error (RMSE) of model monthly standardized anomalies of near-surface soil moisture (SM_s) in experiment CTR with respect to ESA-CCI SM with red indicating a larger RMSE. (b) The difference between RMSE in CTR and IALC (IALC–CTR) with blue (red) indicating a reduced (increased) RMSE. The boxes highlight the three regions Southern Amazon, Lapland and Central Asia with major land cover changes. See Table S2.1 for details of the experiments and Table S2.2 for values in the highlighted regions.

S2.3 Leaf area index results

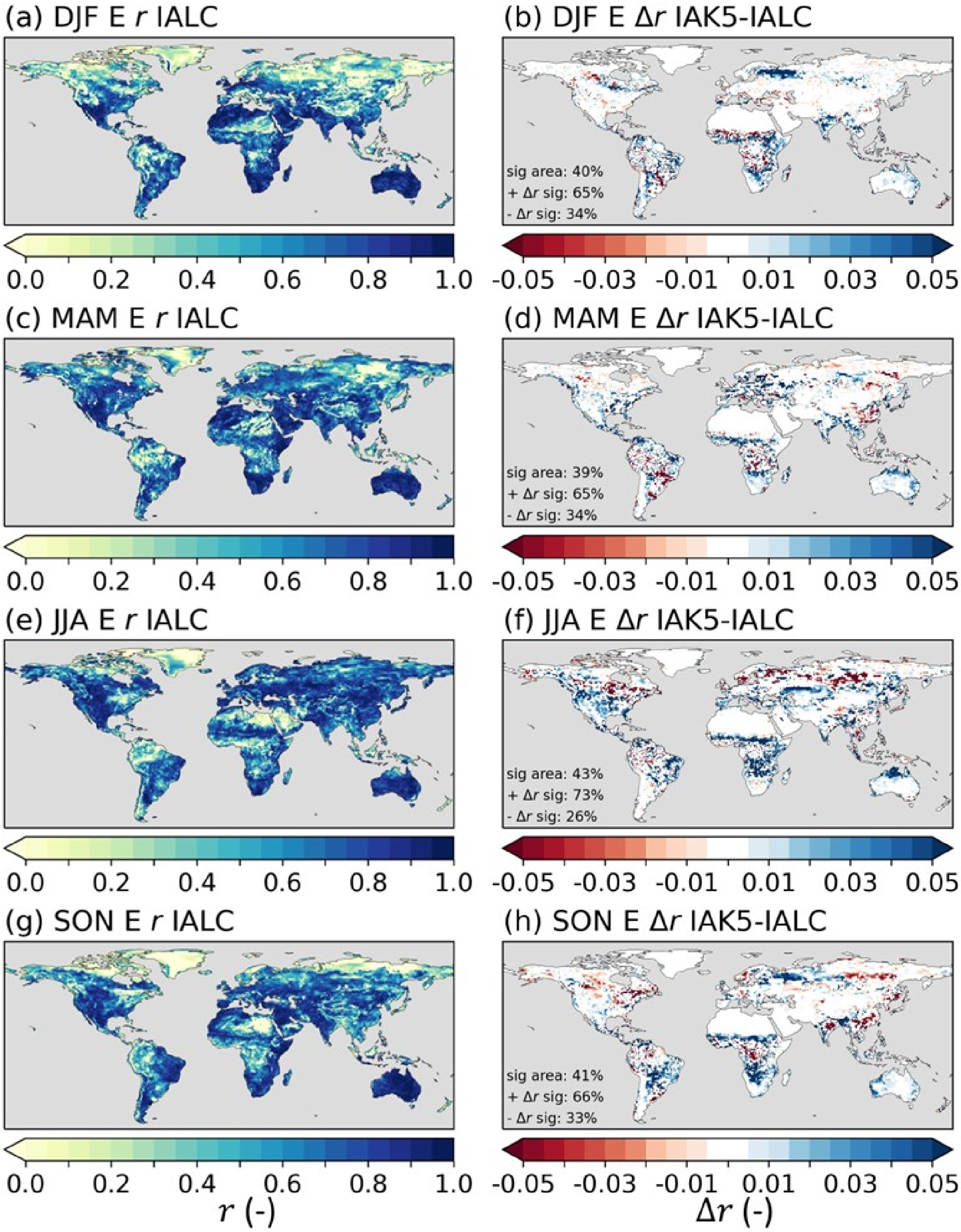

Figure S2.5: (a,c,e,g) Pearson correlation (r) of seasonal anomaly evaporation (E) with respect to DOLCEv3 evaporation in IALC and (b,d,f,h) seasonal correlation difference between IALC and IAK5 (IAK5-IALC). Blue (red) indicates an increased (reduced) correlation in IAK5 compared to IALC, white colors indicate small and/or insignificant differences, and grey indicates no data points. The percentages indicate the areal percentage of significantly changing land points, and the areal percentage of positive and negative Δr for significant points. See Table S2.1 for details of the experiments.

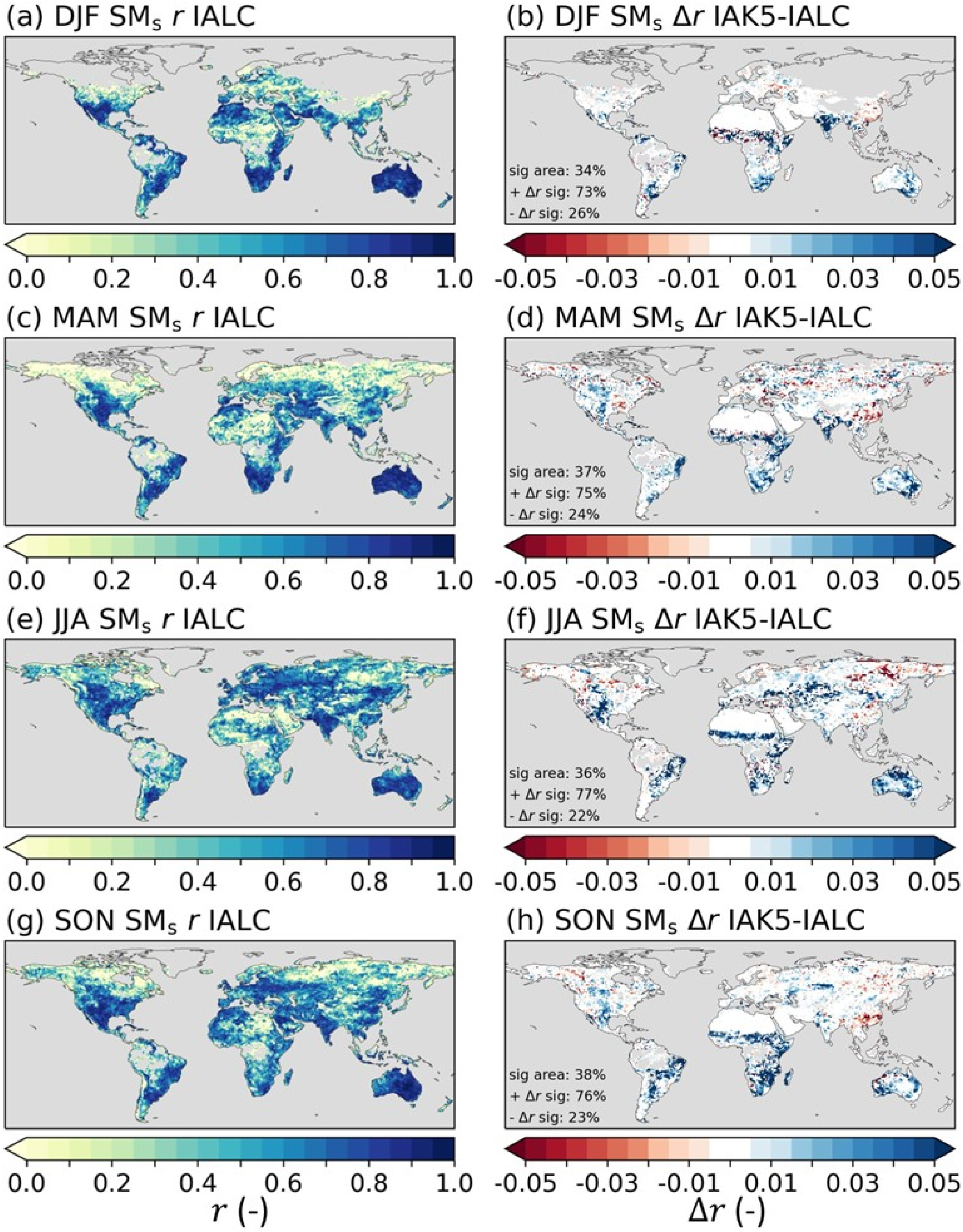

Figure S2.6: (a,c,e,g) Pearson correlation (r) of seasonal anomaly surface soil moisture (SM_s) with respect to ESA-CCI SM in IALC and (b,d,f,h) seasonal correlation difference between IALC and IAK5 (IAK5-IALC). Blue (red) indicates an increased (reduced) correlation in IAK5 compared to IALC, white colors indicate small and/or insignificant differences, and grey indicates no data points. The percentages indicate the areal percentage of significantly changing land points, and the areal percentage of positive and negative Δr for significant points. See Table S2.1 for details of the experiments.

S2.4 Effective vegetation cover results

Table S2.4: Effective vegetation cover k-values for experiments IAK5 and IKAV, with associated RMSE values with respect to the FCover data. Figures associated with the numbers are presented in Fig. 2.10.

Vegetation type	**k IAK5**	**RMSE k IAK5**	**k IAKV**	**RMSE k IAKV**
Crops	0.5	0.042	0.458	0.036
Short grass	0.5	0.031	0.457	0.026
Evergreen Needleleaf trees	0.5	0.098	0.351	0.038
Deciduous needleleaf trees	0.5	0.069	0.381	0.032
Deciduous broadleaf trees	0.5	0.081	0.396	0.053
Evergreen Broadleaf trees	0.5	0.066	0.390	0.036
Tundra	0.5	0.028	0.375	0.018
Bogs and marshes	0.5	0.070	0.419	0.049
Evergreen shrubs	0.5	0.060	0.438	0.045
Deciduous shrubs	0.5	0.037	0.448	0.026

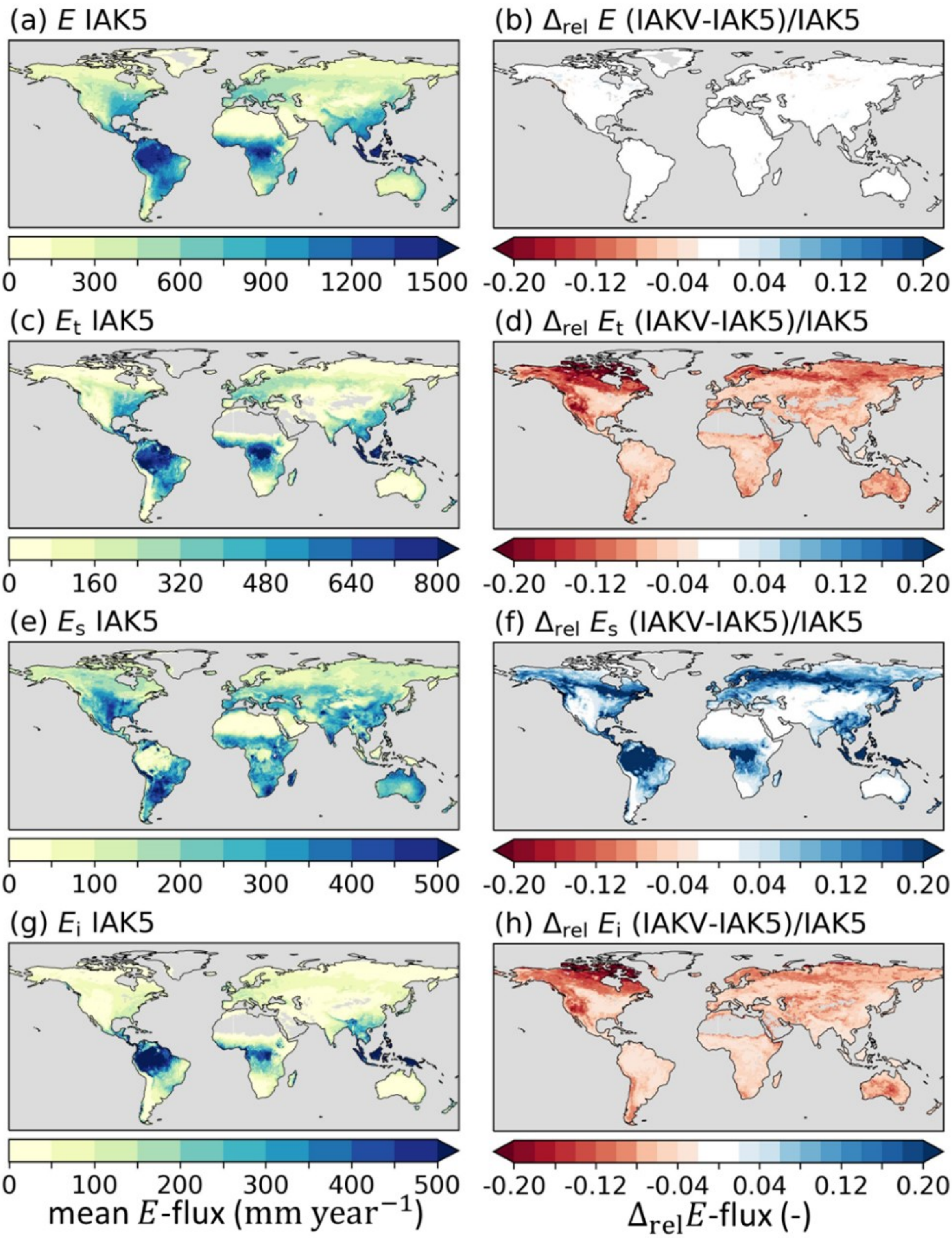

Figure S2.7: Annual mean evaporation fluxes in experiment IAK5 with (a) total evaporation (E), (c) transpiration (E_t), (e) soil evaporation (E_s) and (g) interception evaporation (E_i) and the relative difference between annual mean evaporation fluxes in experiment IAKV and IAK5 ((IAKV-IAK5)/IAK5) for (b) E, (d) E_t, (f) E_s and (h) E_i. Blue (red) indicates an increased (reduced) flux. Grey land areas indicate regions with annual mean E-fluxes < 0.1 mm/year. See Table S2.1 for details of the experiments.

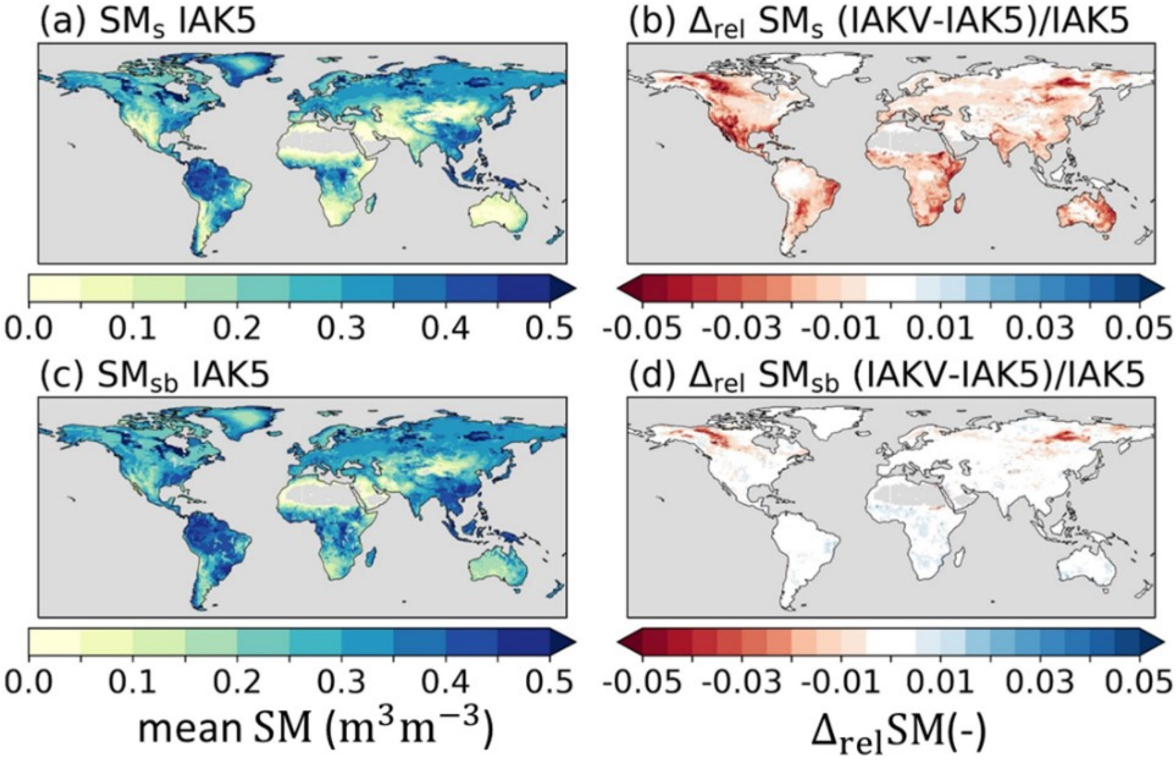

Figure S2.8: Annual mean soil moisture in experiment IAK5 with (a) near-surface soil moisture (SM_s) and (c) subsurface soil moisture (SM_{sb}) and the relative difference between annual mean SM in experiment IAKV and IAK5 ((IAKV-IAK5)/IAK5) for (b) SM_s and (d) SM_{sb}. Blue (red) indicates an increased (reduced) soil moisture. Grey land areas indicate regions with annual mean SM < 0.01 m3/m3. See Table S2.1 for details of the experiments.

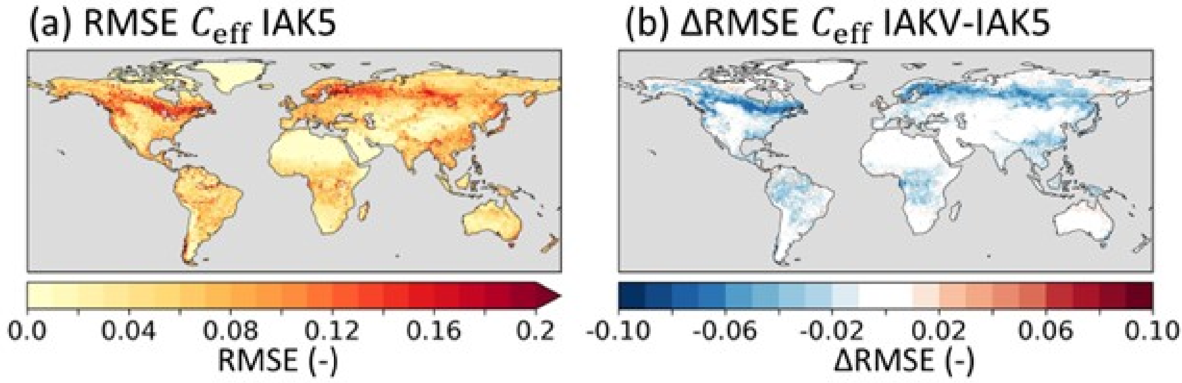

Figure S2.9: (a) Root mean squared error (RMSE) of model monthly effective vegetation cover Ceff in experiment IAK5 with respect to CGLS FCover with red indicating a larger RMSE. (b) The difference between RMSE in IAK5 and IAKV (IAKV-IAK5) with blue (red) indicating a reduced (increased) RMSE. See Table S2.1 for details of the experiments.

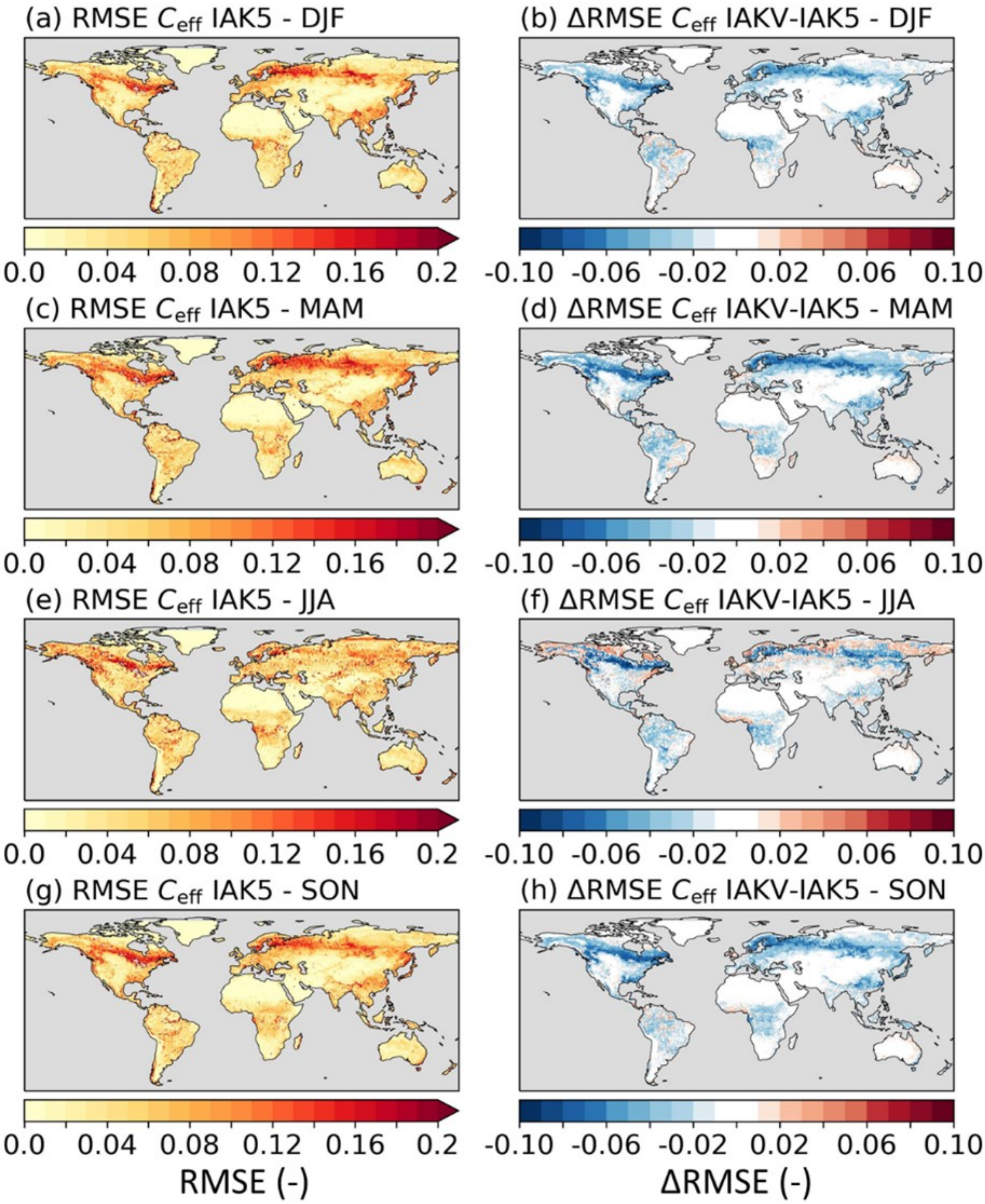

Figure S2.10: Same as Fig. S2.8 for seasonal values.

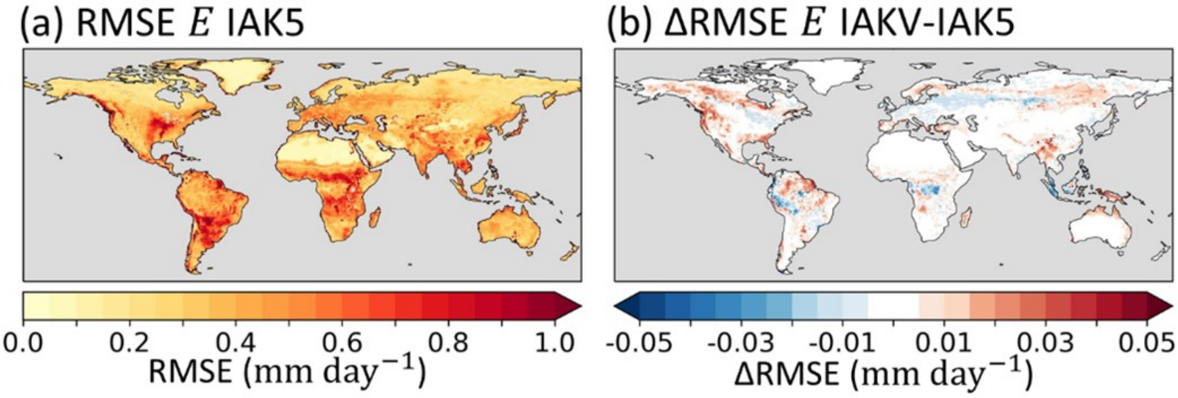

Figure S2.11: (a) Root mean squared error (RMSE) of model monthly evaporation E in experiment IAK5 with respect to DOLCEv3 E with red indicating a larger RMSE. (b) The difference between RMSE in IAK5 and IAKV (IAKV-IAK5) with blue (red) indicating a reduced (increased) RMSE. See Table S2.1 for details of the experiments.

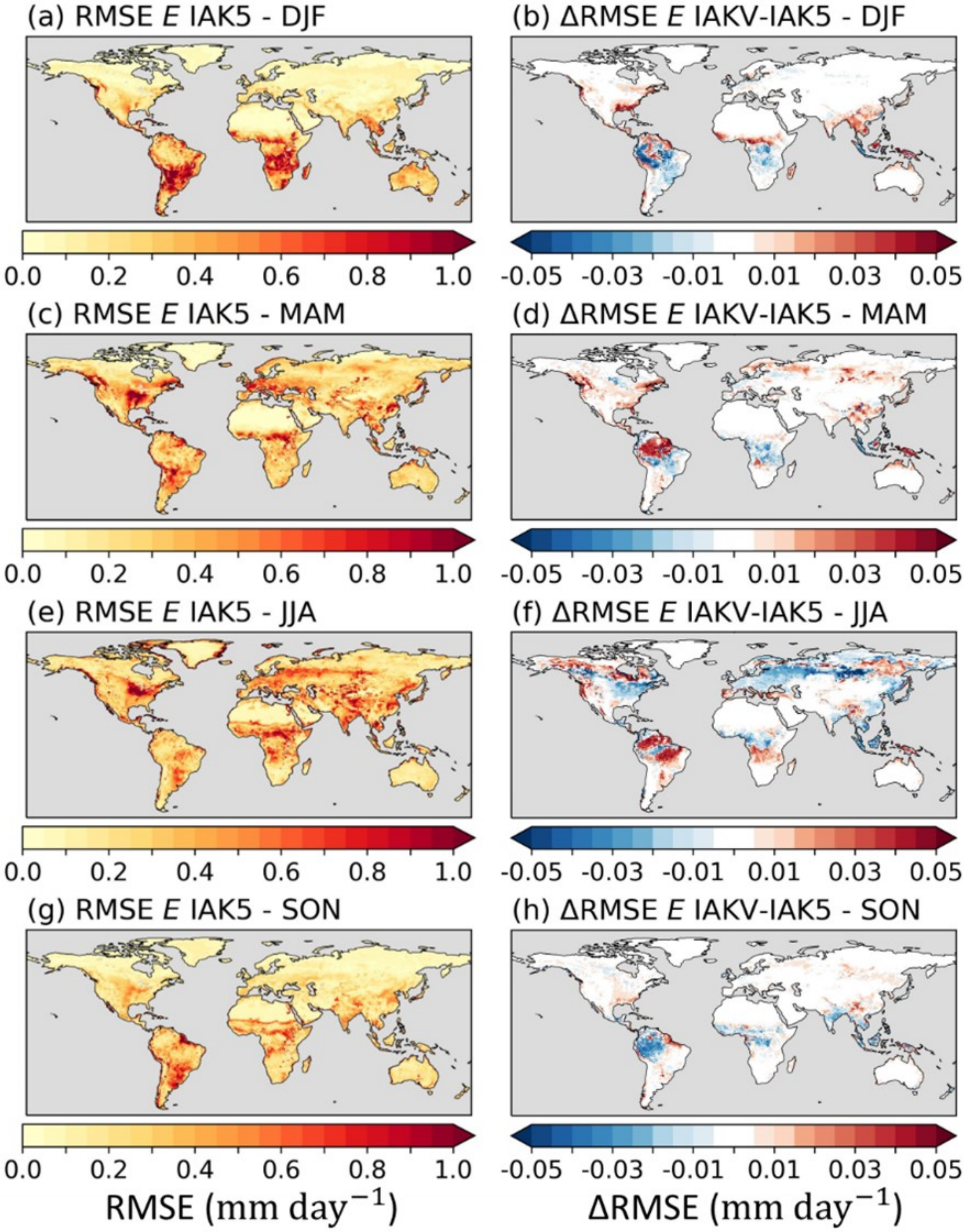

Figure S2.12: Same as Fig. S2.10 for seasonal values

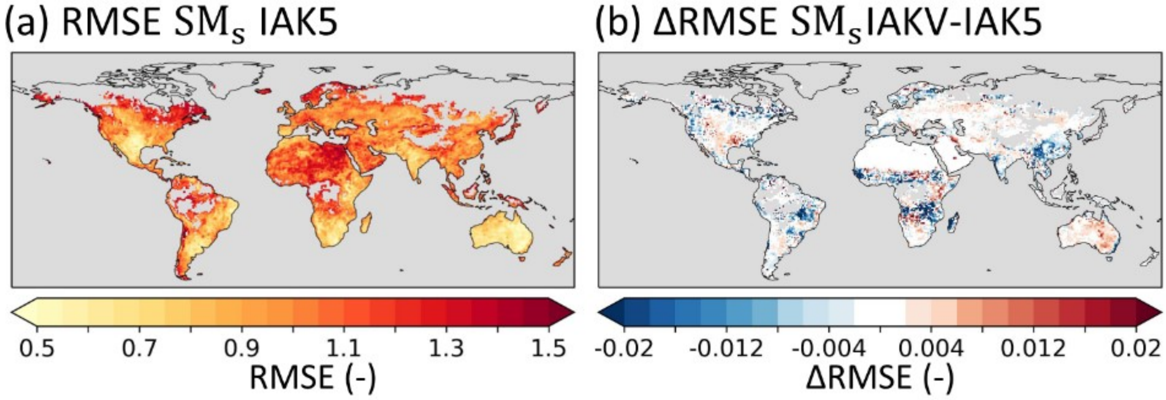

Figure S2.13: (a) Root mean squared error (RMSE) of model monthly standardized anomalies of near-surface soil moisture in experiment IAK5 with respect to ESA-CCI SM with red indicating a larger RMSE. (b) The difference between RMSE in IAK5 and IAKV (IAKV-IAK5) with blue (red) indicating a reduced (increased) RMSE. See Table S2.1 for details of the experiments.

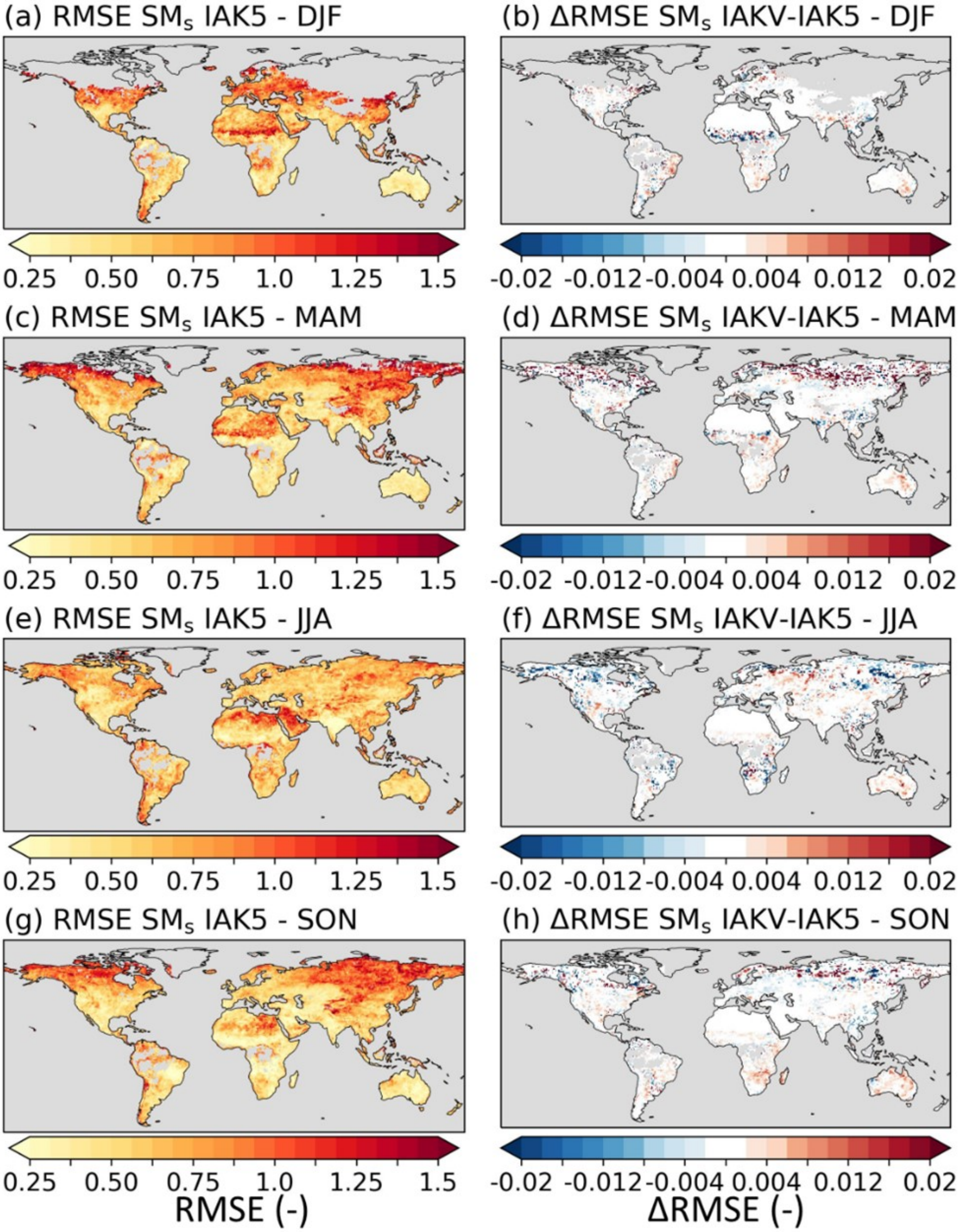

Figure S2.14: Same as Fig. S2.12 for seasonal values

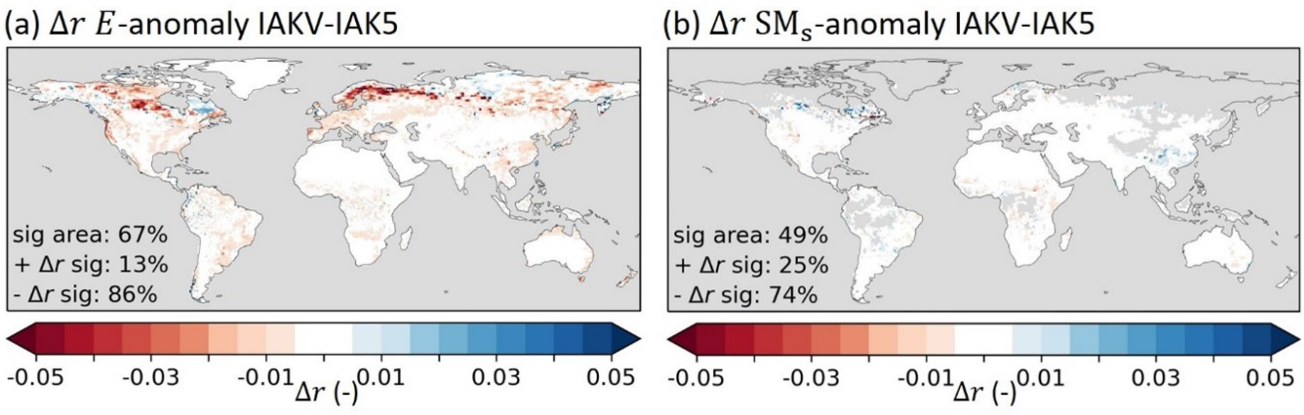

Figure S2.15: Pearson correlation difference between experiment IAK5 and IAKV (IAKV-IAK5) for (a) monthly anomaly total evaporation (E) with respect to DOLCEv3 evaporation and (b) monthly anomaly surface soil moisture ($\mathrm{SM_s}$) with respect to ESA-CCI SM. Blue (red) indicates an increased (reduced) correlation in IAKV compared to IAK5, white indicates small and/or insignificant r differences, and grey indicates no data points. The percentages indicate the areal percentage of significantly changing land points, and the areal percentage of positive and negative Δr for significant points. See Table S2.1 for details of the experiments.

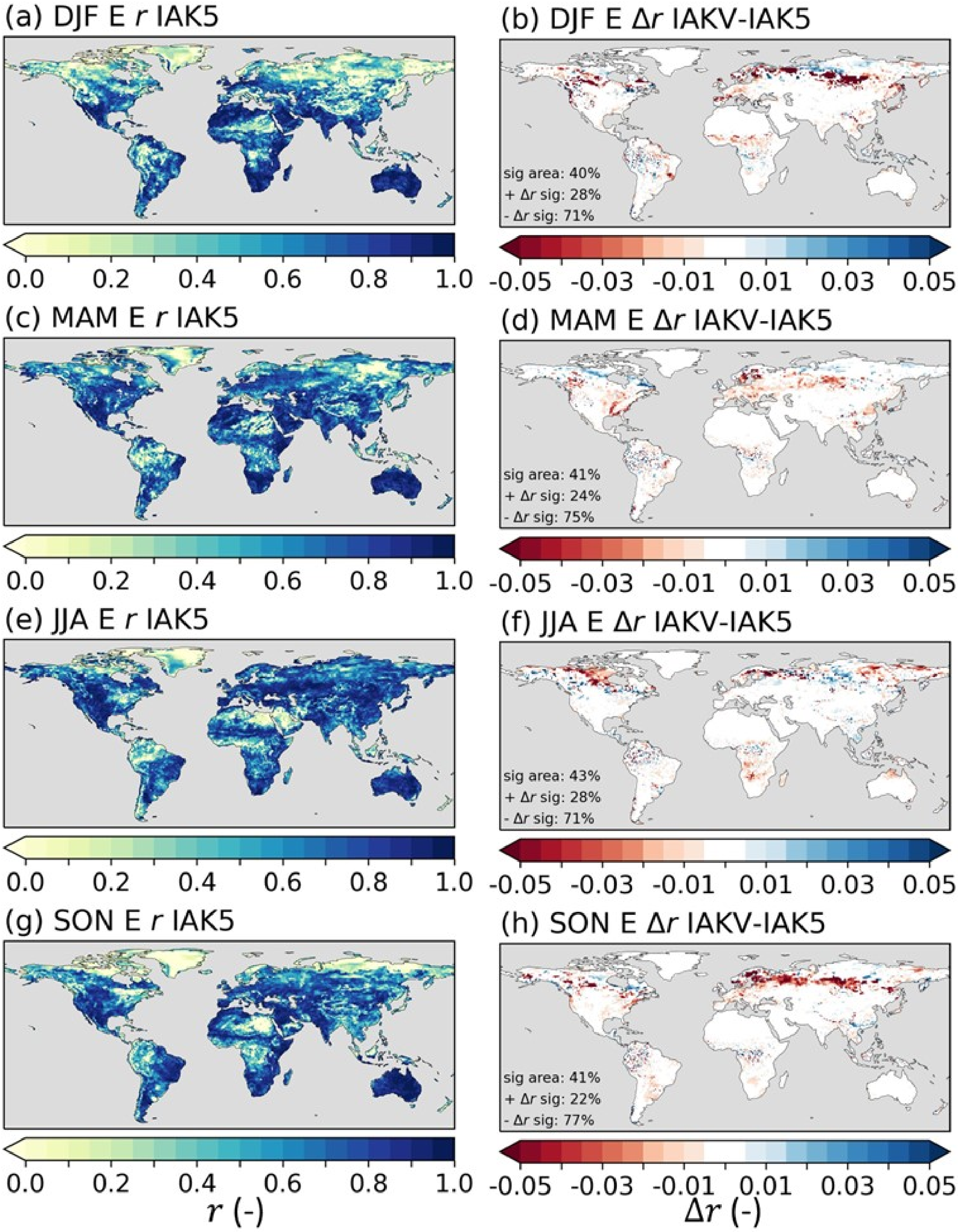

Figure S2.16: (a,c,e,g) Pearson correlation (r) of seasonal anomaly evaporation (E) with respect to DOLCEv3 evaporation in IAK5 and (b,d,f,h) seasonal correlation difference between IAK5 and IAKV (IAKV-IAK5). Blue (red) indicates an increased (reduced) correlation in IAKV compared to IAK5, white colors indicate small and/or insignificant differences, and grey indicates no data points. The percentages indicate the areal percentage of significantly changing land points, and the areal percentage of positive and negative Δr for significant points. See Table S2.1 for details of the experiments.

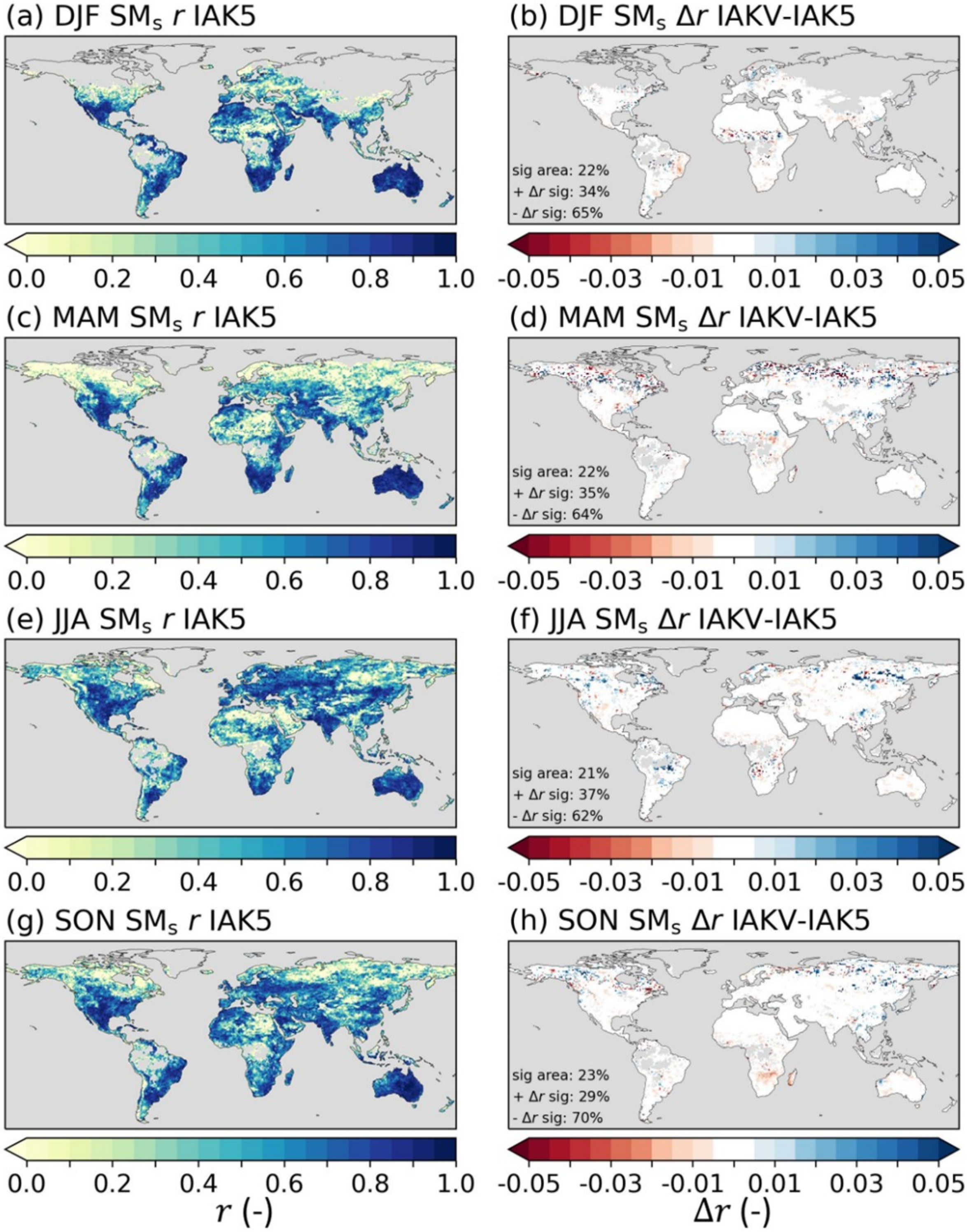

Figure S2.17: (a,c,e,g) Pearson correlation (r) of seasonal anomaly surface soil moisture (SM$_s$) with respect to ESA-CCI SM in IAK5 and (b,d,f,h) seasonal correlation difference between IAK5 and IAKV (IAKV-IAK5). Blue (red) indicates an increased (reduced) correlation in IAKV compared to IAK5, white colors indicate small and/or insignificant differences, and grey indicates no data points. The percentages indicate the areal percentage of significantly changing land points, and the areal percentage of positive and negative Δr for significant points. See Table S2.1 for details of the experiments.

S2.5 Combined results

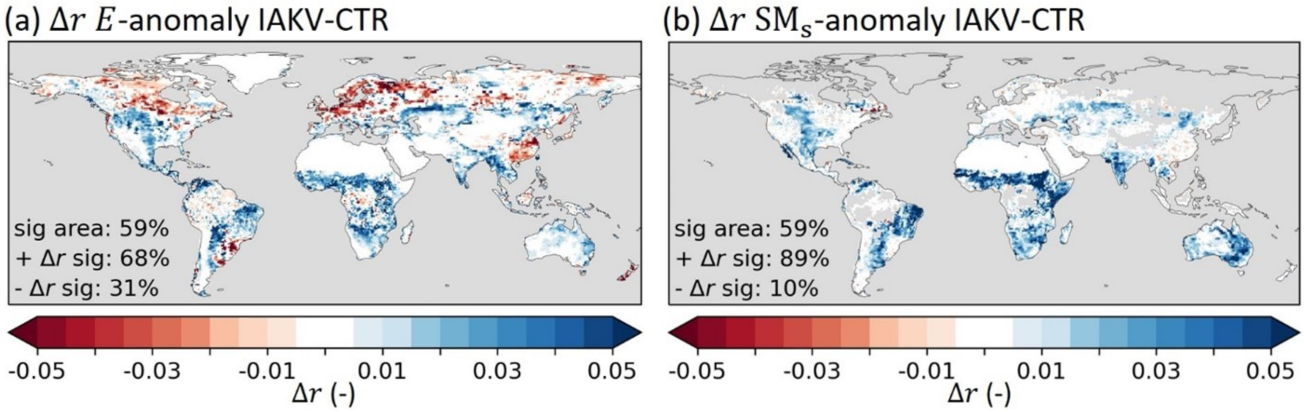

Figure S2.18: Pearson correlation difference between experiment CTR and IAKV (IAKV-CTR) for (a) monthly anomaly total evaporation (E) with respect to DOLCEv3 evaporation and (b) monthly anomaly surface soil moisture (SM_s) with respect to ESA-CCI SM. Blue (red) indicates an increased (reduced) correlation in IAKV compared to CTR, white indicates small and/or insignificant r differences, and grey indicates no data points. The percentages indicate the areal percentage of significantly changing land points, and the areal percentage of positive and negative Δr for significant points. See Table S2.1 for details of the experiments.

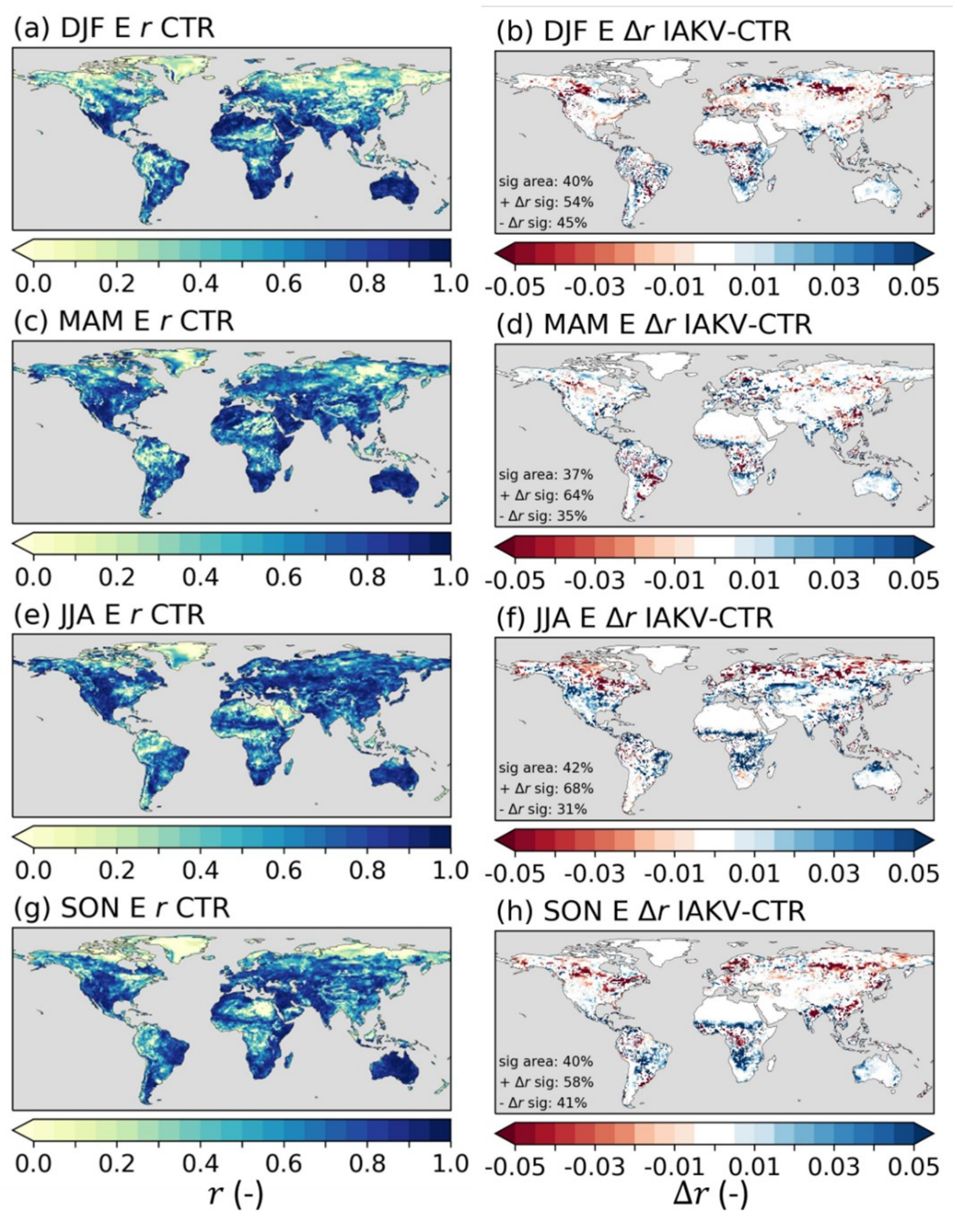

Figure S2.19: (a,c,e,g) Pearson correlation (r) of seasonal anomaly evaporation (E) with respect to DOLCEv3 evaporation in CTR and (b,d,f,h) seasonal correlation difference between CTR and IAKV (IAKV-CTR). Blue (red) indicates an increased (reduced) correlation in IAKV compared to CTR, white colors indicate small and/or insignificant differences, and grey indicates no data points. The percentages indicate the areal percentage of significantly changing land points, and the areal percentage of positive and negative Δr for significant points. See Table S2.1 for details of the experiments.

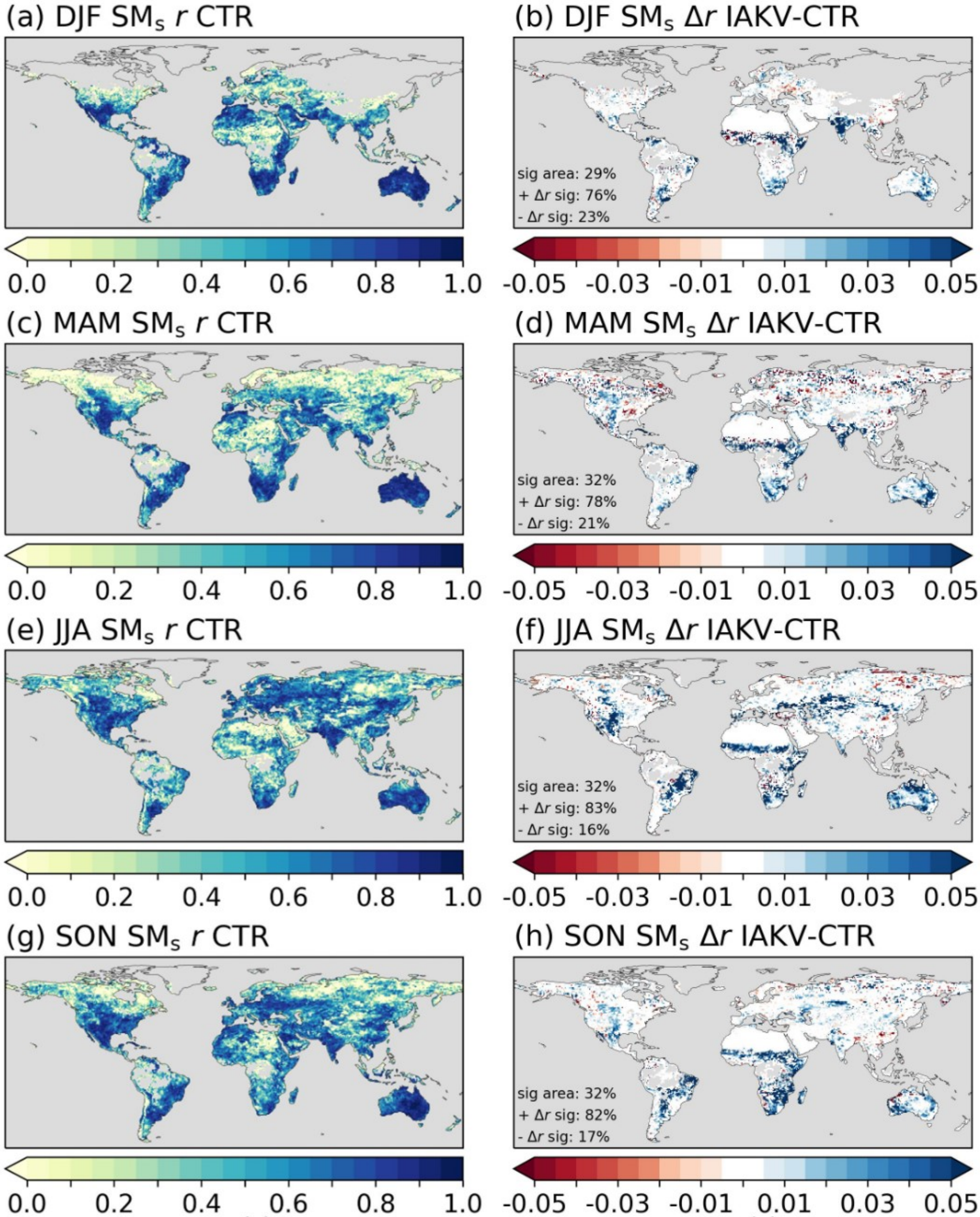

Figure S2.20: (a,c,e,g) Pearson correlation (r) of seasonal anomaly surface soil moisture (SM_s) with respect to ESA-CCI SM in CTR and (b,d,f,h) seasonal correlation difference between CTR and IAKV (IAKV-CTR). Blue (red) indicates an increased (reduced) correlation in IAKV compared to CTR, white colors indicate small and/or insignificant differences, and grey indicates no data points. The percentages indicate the areal percentage of significantly changing land points, and the areal percentage of positive and negative Δr for significant points. See Table S2.1 for details of the experiments.

S2.6 Data and code availability

The scripts underlying this chapter are available on https://github.com/fvanoorschot/python_scripts_vanoorschot2023 or https://doi.org/10.5281/zenodo.8254556. Data underlying this chapter is available on https://doi.org/10.5281/zenodo.8307861.

Supporting information for chapter 3: Climate-controlled root zone parameters in land surface models

S3.1 Catchment information

Table S3.1: Study catchment characteristics (Australian Bureau of Meteorology; http://www.bom.gov.au/water/hrs/). Soil type is based on the FAO soil map of the world (FAO, 2003) and vegetation characteristics from GLCC1.2 (ECMWF, 2016) with T_L and T_H the dominant low and high vegetation types and C_L and C_H the fractional coverage of low and high vegetation.

Catchment	**Station ID**	**Coordinates**	**Climate region**	**Area (km^2)**	**Soil type**	$\mathbf{T_L}$	$\mathbf{T_H}$	$\mathbf{C_L}$ **(-)**	$\mathbf{C_H}$ **(-)**
East Alligator River (EA)	G8210010	133.332°E, 12.717°S	Tropical	2398	Coarse	Tall grass	Interrupted forest	0.68	0.32
East Baines River (EB)	G8110004	130.034°E, 15.766°S	Tropical	2443	Coarse	Semi-desert		1.00	0.00
Gregory River (G)	912101A	139.252°E, 18.643°S	Tropical	12652	Medium fine	Short grass		1.00	0.00
Herbert River (He)	116006B	145.922°E, 18.491°S	Tropical	7487	Medium fine	Tall grass	Evergreen broadleaf	0.01	0.99
Mitchell River (Mi)	919003A	144.290°E, 16.472°S	Tropical	7734	Coarse	Tall grass	Interrupted forest	0.43	0.57
Normanby River (No)	105101A	144.839°E, 15.281°S	Tropical	2306	Coarse	Tall grass	Interrupted forest	0.01	0.99
Wenlock River (W)	925001A	142.638°E, 12.454°S	Tropical	3290	Medium fine		Interrupted forest	0.00	1.00
Abercrombie River (A)	412028	149.325°E, 33.955°S	Temperate	2631	Medium	Crops, mixed farming	Interrupted forest	0.23	0.76
Dogwood Creek (D)	422202B	150.179°E, 26.709°S	Temperate	2882	Medium fine	Tall grass	Evergreen broadleaf	0.14	0.86
Murrumbidgee River (Mu)	410761	149.101°E, 35.540°S	Temperate	5158	Medium fine	Tall grass	Interrupted forest	0.16	0.84
Namoi River (Na)	419005	150.778°E, 30.678°S	Temperate	2532	Medium	Crops, mixed farming	Interrupted forest	0.33	0.67
Paroo River (P)	424201A	144.786°E, 28.689°S	Temperate	22885	Medium	Semi-desert		1.00	0.00
Avoca River (Av)	408200	143.299°E, 36.438°S	Mediterranean	2677	Medium	Crops, mixed farming	Interrupted forest	0.79	0.21
Kent River (K)	604053	117.087°E, 34.888°S	Mediterranean	1786	Coarse	Crops, mixed farming	Interrupted forest	0.65	0.35
Reedy Creek (R)	403209A	146.345°E, 36.332°S	Mediterranean	5506	Medium fine	Crops, mixed farming	Evergreen broadleaf	0.02	0.98

Table S3.2: Hydrological characteristics of the study catchments with long-term (1973–2010) annual mean values for precipitation ($\overline{P}$), discharge ($\overline{Q}$) and potential evaporation ($\overline{E_{\mathrm{p}}}$), aridity index ($I_{\mathrm{A}}$), seasonality index ($I_{\mathrm{S}}$), time-lag between maximum monthly mean precipitation and potential evaporation (ϕ) and root zone storage capacity estimates from the memory method ($S_{\mathrm{r,MM}}$) and in the HTESSEL CTR model ($S_{\mathrm{r,CTR}}$).

Catchment	$\overline{\mathbf{P}}$ **(mm/year)**	$\overline{\mathbf{Q}}$ **(mm/year)**	$\overline{\mathbf{E}_{\mathrm{p}}}$ **(mm/year)**	$\mathbf{I}_{\mathrm{A}}$ **(-)**	$\mathbf{I}_{\mathrm{S}}$ **(-)**	ϕ	$\mathbf{S}_{\mathrm{r,MM}}$ **(mm)**	$\mathbf{S}_{\mathrm{r,CTR}}$ **(mm)**
EA	1539	586	953	1.31	0.97	3	389	535
EB	879	134	745	2.53	0.99	3	300	535
G	509	55	453	3.96	0.95	1	194	513
He	1140	326	814	1.46	0.70	2	409	725
Mi	854	251	603	2.05	0.89	2	410	535
No	1207	288	920	1.40	0.85	2	722	535
W	1577	472	1105	1.10	0.95	3	633	725
A	787	94	693	1.55	0.07	0	208	566
D	661	24	637	2.69	0.38	0	266	725
Mu	588	59	530	2.04	0.08	2	205	725
Na	802	84	718	1.76	0.26	0	165	566
P	417	26	392	4.38	0.37	1	125	566
Av	505	8	497	2.69	0.25	5	160	566
K	889	41	848	1.36	0.50	6	315	535
R	1243	109	1133	1.02	0.26	6	487	725

S3.2 Model results long-term annual mean fluxes

Table S3.3: Long-term (1975–2010) annual mean reference and modeled (HTESSEL CTR and MD models) precipitation ($\overline{P}$), discharge ($\overline{Q}$) and evaporation ($\overline{E}$) fluxes in the study catchments.

	$\overline{\textbf{P}}$ (mm/year)	$\overline{\textbf{Q}}$ (mm/year)			$\overline{\textbf{E}}$ (mm/year)			
Catchment	**GSWP-3**	**Station observations**	**CTR**	**MD**	**Water balance**	**FLUXCOM**	**CTR**	**MD**
EA	1429	590	423	436	839	753	1002	989
EB	788	132	176	167	656	587	612	621
G	514	50	19	42	464	434	498	471
He	1051	309	198	236	742	694	847	808
Mi	1155	231	256	264	923	622	891	883
No	1405	270	570	597	1135	765	827	801
W	1538	455	675	675	1082	900	856	857
A	769	87	69	85	682	634	702	682
D	674	25	34	36	648	586	638	635
Mu	686	60	77	96	626	464	615	590
Na	889	84	96	110	805	658	790	778
P	394	24	18	22	370	333	372	371
Av	531	7	6	20	524	449	529	511
K	1066	41	200	200	1024	730	867	866
R	1056	98	305	312	958	709	755	749

Table S3.4: Percent biases of modeled (HTESSEL CTR and MD models) long-term (1975–2010) annual mean discharge ($\overline{Q}$) and evaporation ($\overline{E}$) with for $\overline{Q}$ station observations as reference data and for $\overline{E}$ water balance and FLUXCOM as reference data.

	$\overline{\textbf{Q}}$ (mm/year)		$\overline{\textbf{E}}$ (mm/year)			
	Station observations		**Water balance**		**FLUXCOM**	
Catchment	**CTR**	**MD**	**CTR**	**MD**	**CTR**	**MD**
EA	-28%	-26%	19.4%	17.9%	32.9%	31.3%
EB	33%	26%	-6.7%	-5.3%	4.3%	5.7%
G	-63%	-14%	7.3%	1.5%	14.8%	8.6%
He	-36%	-24%	14.2%	8.9%	22.0%	16.3%
Mi	11%	14%	-3.5%	-4.4%	43.2%	41.9%
No	111%	121%	-27.1%	-29.4%	8.0%	4.6%
W	48%	48%	-20.9%	-20.8%	-4.9%	-4.8%
A	-20%	-2%	3.0%	0.0%	10.7%	7.6%
D	34%	41%	-1.6%	-2.0%	8.8%	8.4%
Mu	28%	60%	-1.7%	-5.7%	32.7%	27.3%
Na	14%	31%	-1.8%	-3.4%	20.1%	18.2%
P	-25%	-6%	0.6%	0.2%	11.8%	11.4%
Av	-9%	196%	0.9%	-2.4%	17.6%	13.8%
K	386%	385%	-15.4%	-15.4%	18.7%	18.6%
R	211%	217%	-21.2%	-21.8%	6.5%	5.6%

S3.3 Model results monthly discharge

Table S3.5: Model performance based on monthly modeled (HTESSEL CTR and MD models) discharge fluxes compared to station observations with Pearson correlation (r) and variability ($\alpha = \sigma_{\mathrm{mod}}/\sigma_{\mathrm{obs}}$) for monthly seasonal climatology of discharge fluxes for the time series 1975–2010 in the study catchments. For both r and α a value of 1 corresponds to a perfect model fit. The significance test of the MD improvements compared to CTR is represented by ** (passing 5% level) and * (passing 10% level) and additionally P-values are provided for the cases that MD improves compared to CTR.

	Monthly seasonal climatology					
	r (-)			**α (-)**		
Catchment	**CTR**	**MD**	**P-value**	**CTR**	**MD**	**P-value**
EA	0.63	0.77**	0.001	0.79	0.87**	0.045
EB	0.60	0.92**	<0.001	0.73	1.11*	0.069
G	0.96	0.98	0.337	0.46	1.14**	0.05
He	0.98	0.99	0.281	0.58	0.63*	0.10
Mi	0.83	0.87	0.178	0.84	1.00**	0.003
No	0.91	0.82	-	1.71	1.55**	0.022
W	0.99	0.99	-	1.31	1.37	-
A	0.94	0.99	0.206	0.39	0.84**	<0.001
D	0.74	0.73	-	1.47	1.39**	0.001
Mu	0.90	0.97	0.074	0.63	1.49	-
Na	0.21	0.62**	0.022	0.76	0.72	-
P	0.92	0.98**	0.002	0.77	1.03**	0.023
Av	0.88	0.95	0.319	0.55	3.64	-
K	0.75	0.95**	<0.001	3.77	5.22	-
R	0.96	0.98**	0.018	1.72	2.20	-

Table S3.6: Same as Table S3.3 for inter-annual anomalies of monthly discharge.

	Inter-annual anomalies					
	r (-)			**α (-)**		
Catchment	**CTR**	**MD**	**P-value**	**CTR**	**MD**	**P-value**
EA	0.61	0.65**	0.002	1.02	1.07	-
EB	0.52	0.71**	<0.001	0.79	1.06**	<0.001
G	0.85	0.86	0.39	0.47	1.65	-
He	0.86	0.87	0.342	0.68	0.74**	<0.001
Mi	0.64	0.71**	<0.001	0.93	1.09	
No	0.86	0.80	-	1.52	1.39**	<0.001
W	0.85	0.85	-	1.35	1.39	-
A	0.83	0.90**	0.03	0.50	0.85**	<0.001
D	0.77	0.78**	<0.001	0.91	0.93**	0.006
Mu	0.88	0.94**	0.007	0.84	1.45	-
Na	0.72	0.84**	<0.001	0.65	0.84**	<0.001
P	0.78	0.79	0.421	0.81	1.23	-
Av	0.67	0.71	0.255	0.81	3.39	-
K	0.62	0.76**	0.002	2.55	3.47	-
R	0.83	0.89**	<0.001	1.72	1.99	-

Figure S3.1: Monthly anomalies (left) and monthly seasonal climatology (right) of modeled discharge with the HTESSEL CTR and MD models compared to discharge from station observations in the study catchments (Table S1). Monthly anomaly discharge is presented for the time series 1990-2010 and monthly seasonal climatology is based on the time series of 1975-2010. Note that this figure continues on the next two pages.

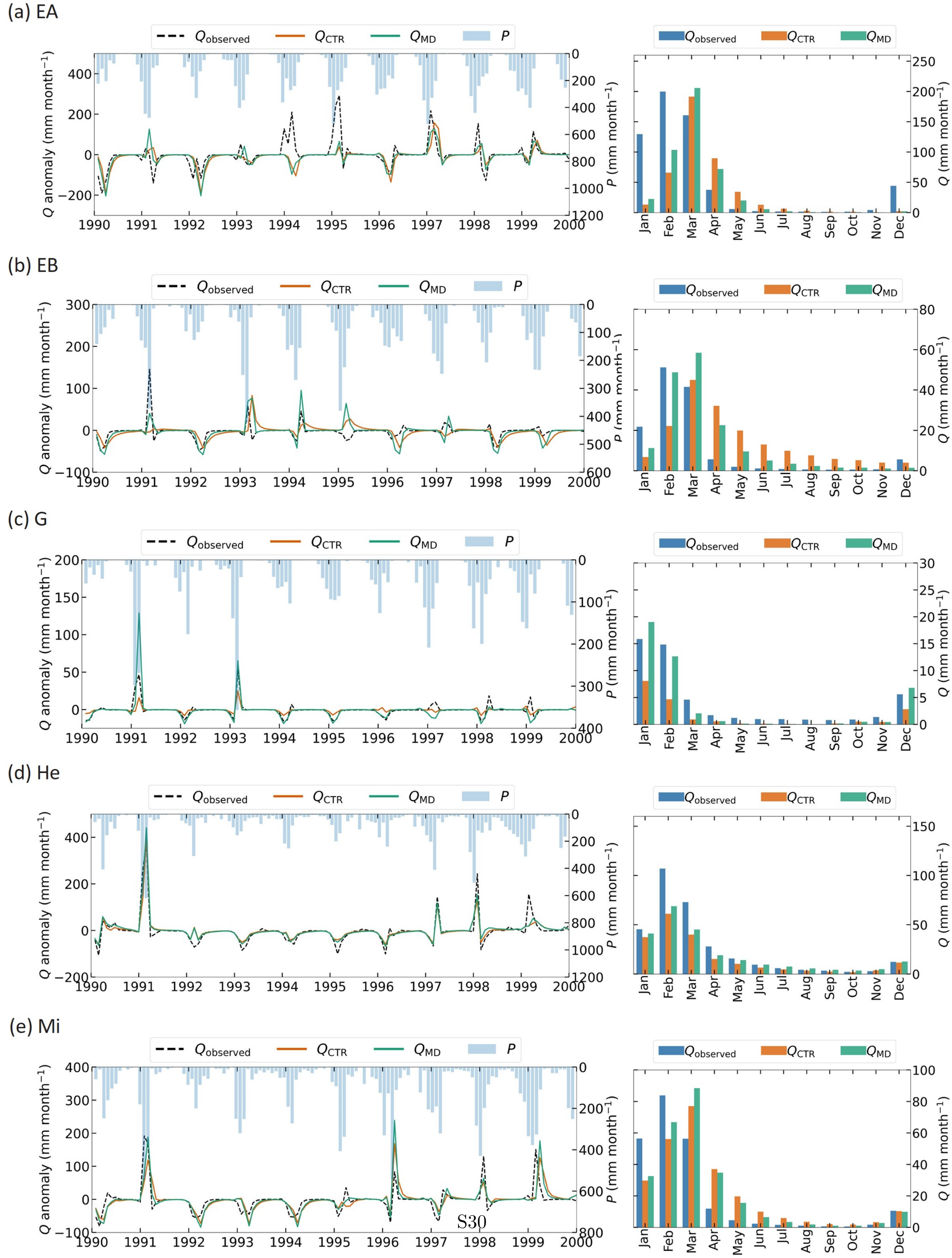

(f) No

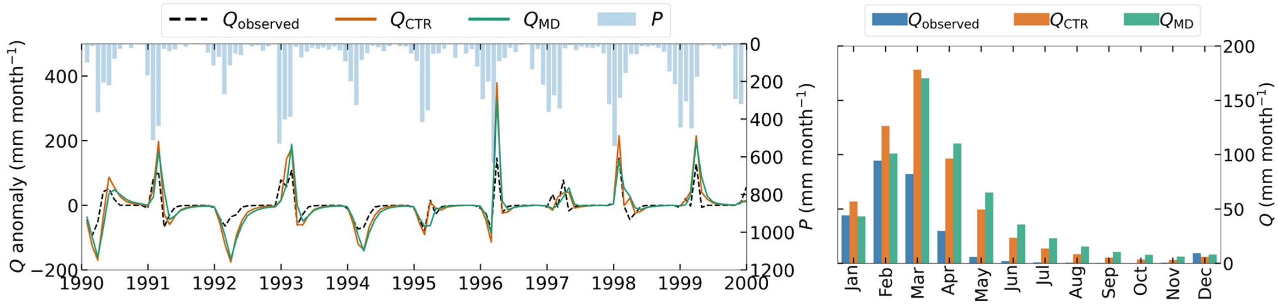

(g) W

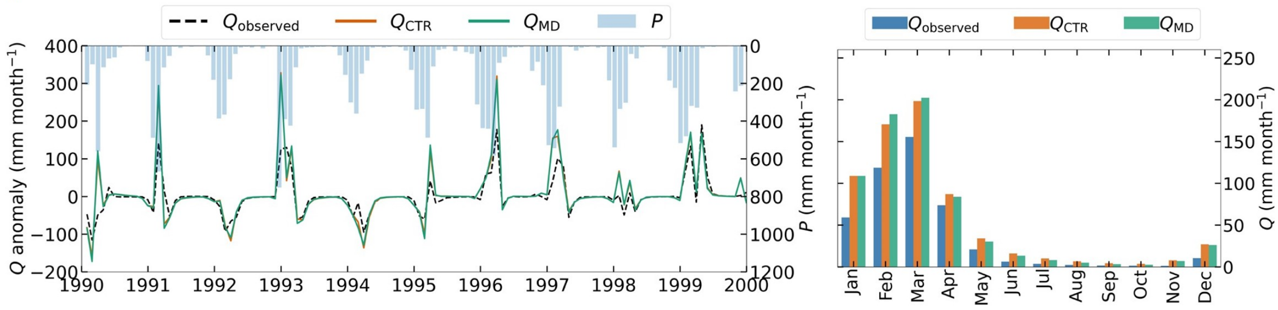

(h) A

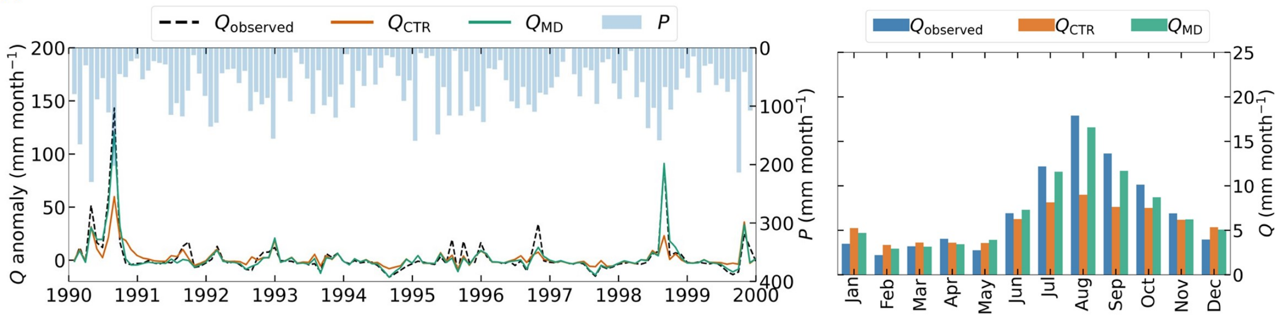

(i) D

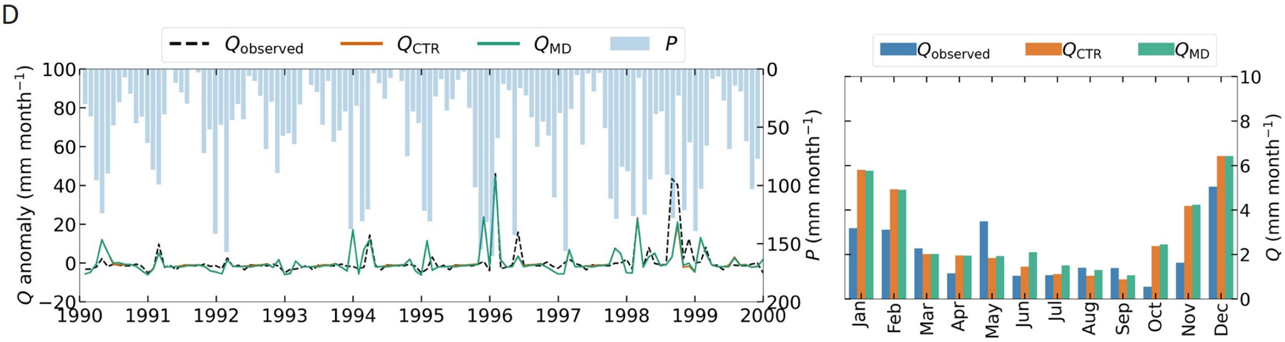

(j) Na

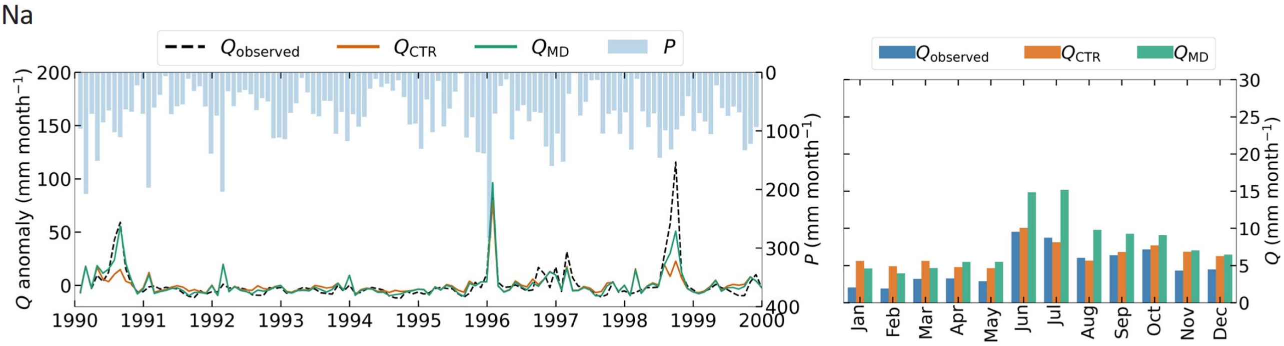

(k) Mu

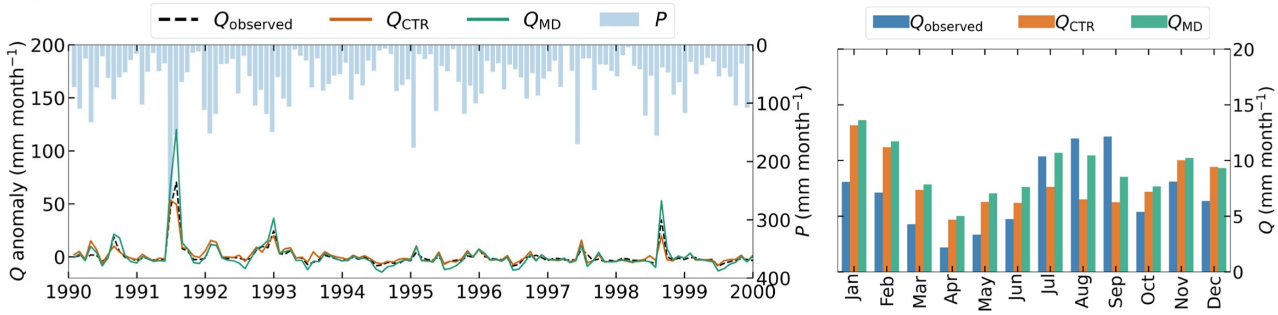

(l) P

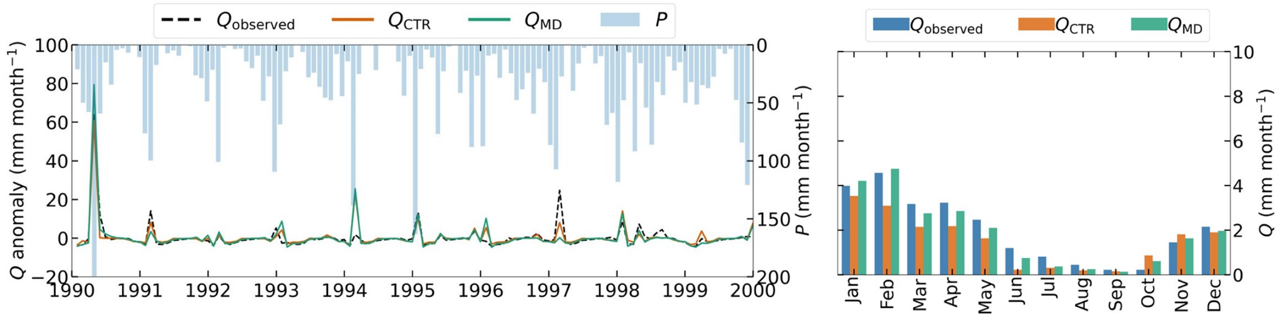

(m) Av

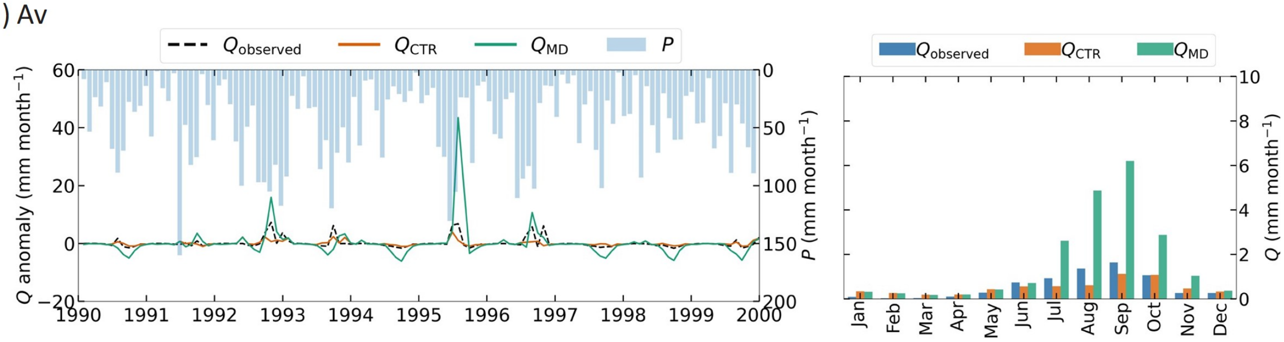

(n) K

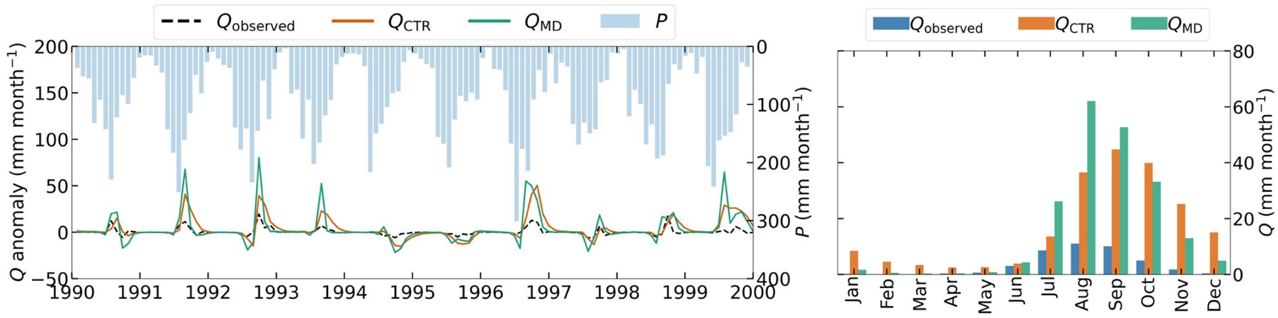

(o) R

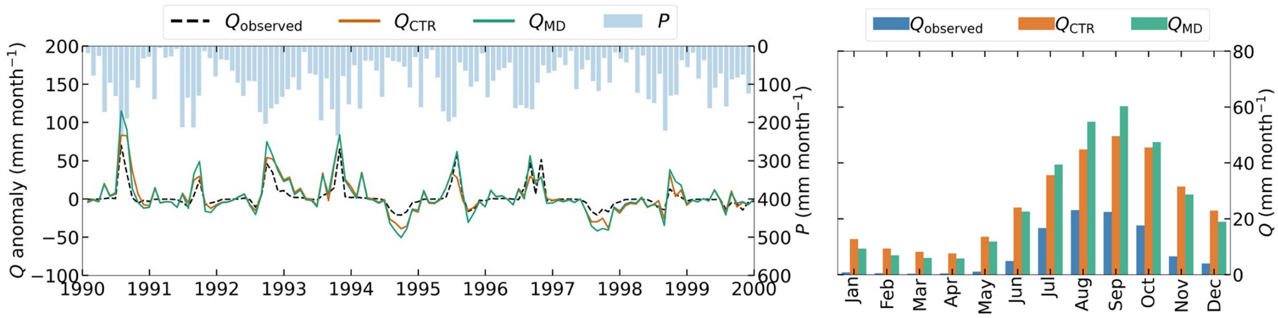

S3.4 Model results monthly evaporation

Table S3.7: Model performance based on monthly modeled (HTESSEL CTR and MD models) evaporation fluxes compared to FLUXCOM-WB with Pearson correlation (r) and variability ($\alpha = \sigma_{\mathrm{mod}}/\sigma_{\mathrm{obs}}$) for monthly seasonal climatology evaporation for the time series 1975–2010 in the study catchments. For both r and α a value of 1 corresponds to a perfect model fit. The significance test of the MD improvements compared to CTR is represented by ** (passing 5% level) and * (passing 10% level) and additionally P-values are provided for the cases that MD improves compared to CTR.

	Monthly seasonal climatology					
	r (-)			**α (-)**		
Catchment	**CTR**	**MD**	**P-value**	**CTR**	**MD**	**P-value**
EA	0.99	0.98	-	1.22	1.23	-
EB	0.99	0.99	-	1.18	1.17**	0.004
G	0.99	0.99	-	1.40	1.45	-
He	0.99	0.98	-	0.88	0.97**	0.015
Mi	0.98	0.97	-	0.69	0.69	-
No	0.98	0.99	0.154	0.65	0.68**	0.002
W	0.98	0.97	-	0.86	0.86	-
A	0.99	0.98	-	0.96	0.94	-
D	0.99	0.99	-	0.73	0.72	-
Mu	0.99	0.98	-	0.87	0.82	-
Na	1.00	1.00	-	0.79	0.75	-
P	0.98	0.97	-	0.77	0.76	-
Av	0.94	0.89	-	1.07	1.14	-
K	0.51	0.53**	0.031	0.60	0.64**	<0.001
R	0.99	0.99	-	0.74	0.74	0.486

Table S3.8: Same as Table S3.4 for inter-annual anomalies of monthly evaporation.

	Inter-annual anomalies					
	r (-)			**α (-)**		
Catchment	**CTR**	**MD**	**P-value**	**CTR**	**MD**	**P-value**
EA	0.81	0.81	-	2.12	2.16	-
EB	0.70	0.70	-	2.57	2.57*	0.072
G	0.82	0.83**	0.001	3.30	3.40	-
He	0.71	0.75**	<0.001	1.72	1.89	-
Mi	0.83	0.83	-	1.36	1.38	-
No	0.85	0.83	-	1.19	1.23	-
W	0.84	0.84	-	1.20	1.21	-
A	0.86	0.86*	0.064	1.88	2.05	-
D	0.84	0.84	-	1.52	1.64	-
Mu	0.82	0.85**	<0.001	1.32	1.50	-
Na	0.79	0.80**	0.05	1.88	2.17	-
P	0.73	0.73	0.281	2.92	3.05	-
Av	0.82	0.82	0.222	2.28	2.40	-
K	0.66	0.67	0.149	2.29	2.31	-
R	0.86	0.85	-	1.46	1.51	-

Figure S3.2: Monthly anomalies (left) and monthly seasonal climatology (right) of modeled evaporation with the HTESSEL CTR and MD models compared to FLUXCOM-WB evaporation in the study catchments (Table S3.1). Monthly anomaly evaporation is presented for the time series 1990- 2010 and monthly seasonal climatology is based on the time series of 1975-2010. Note that this figure continues on the next two pages.

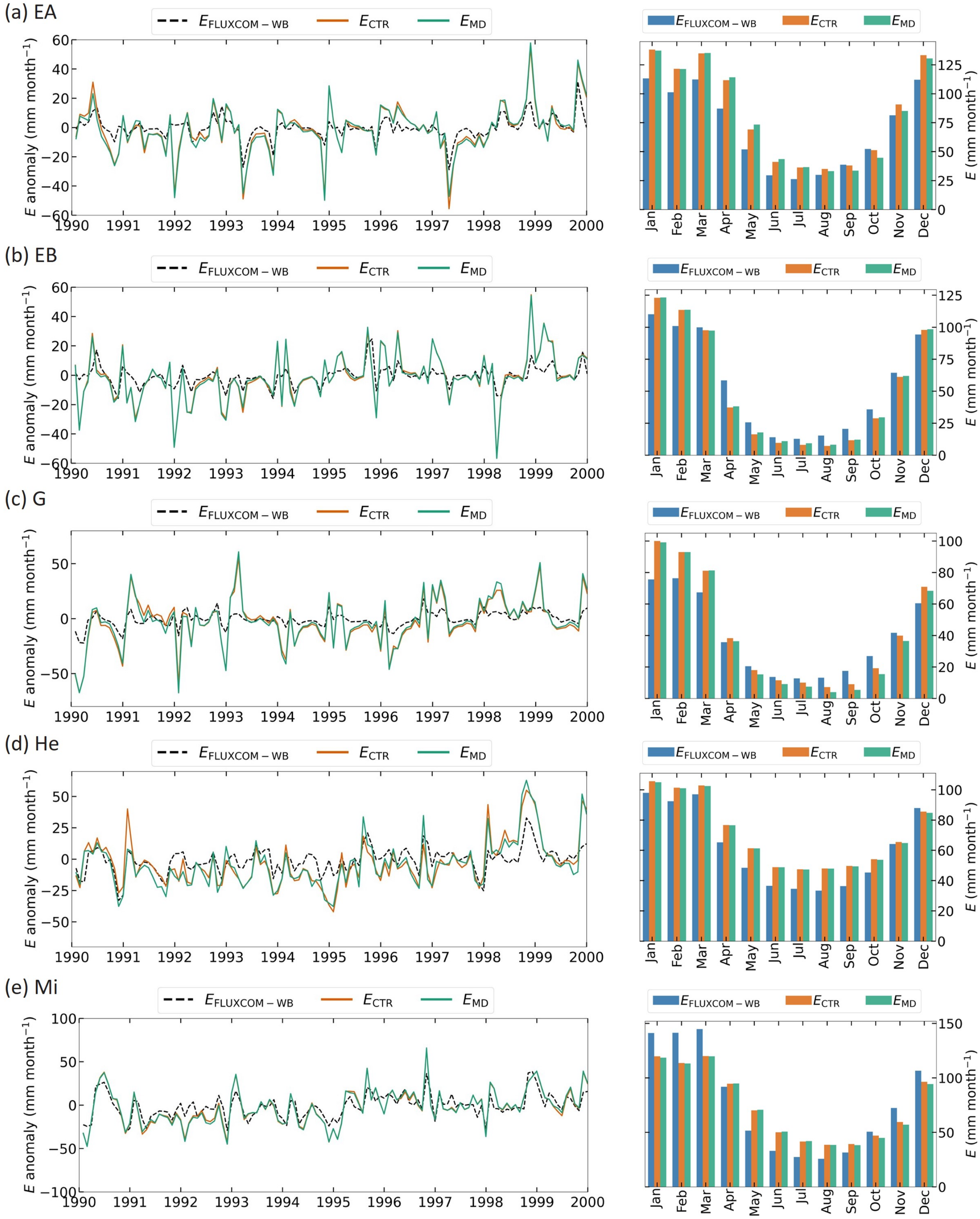

(f) No

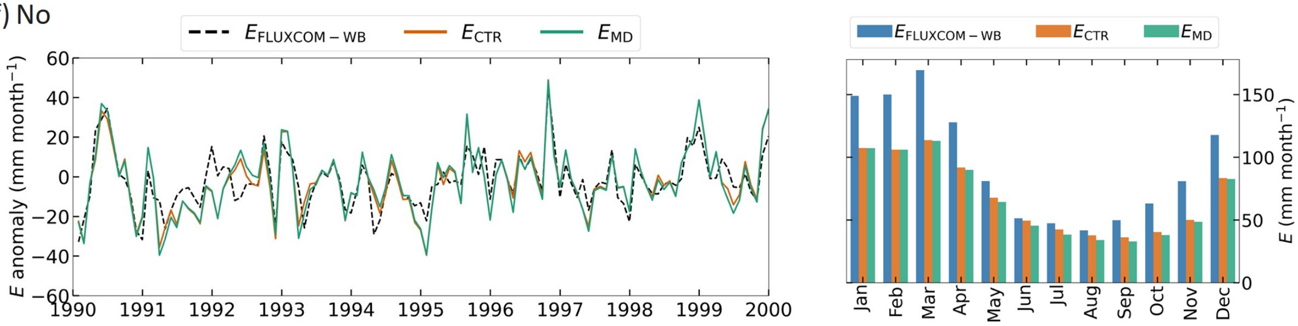

(g) W

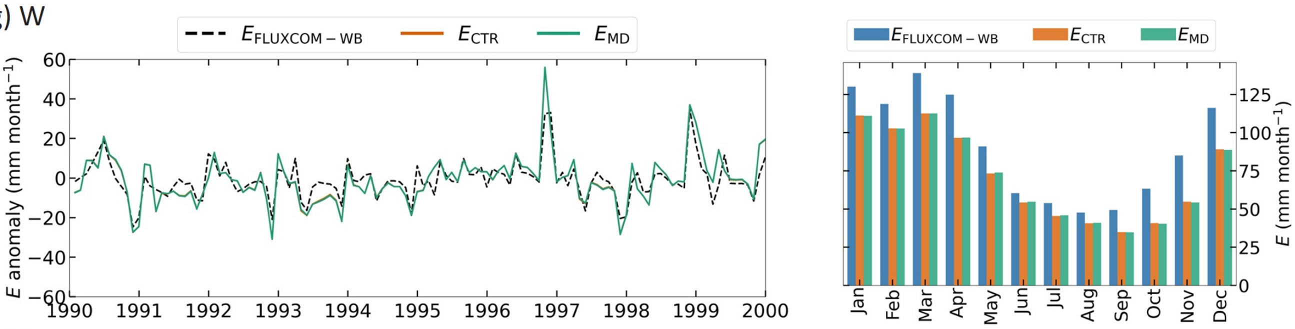

(h) A

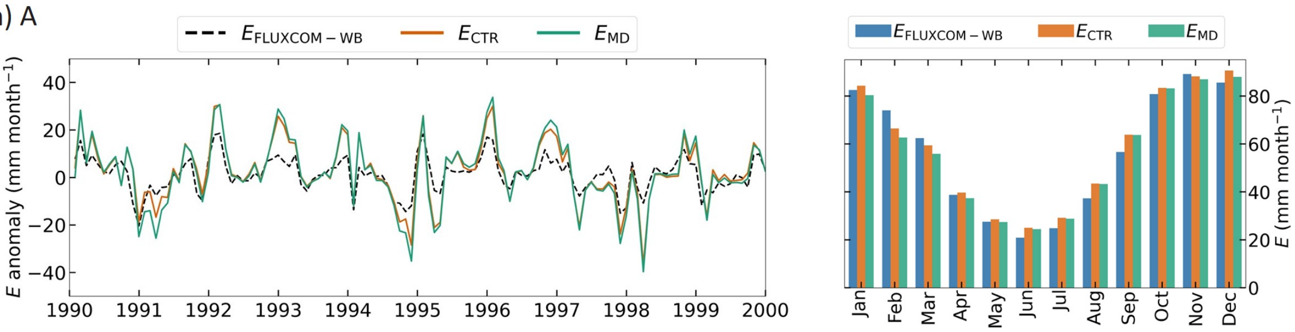

(i) D

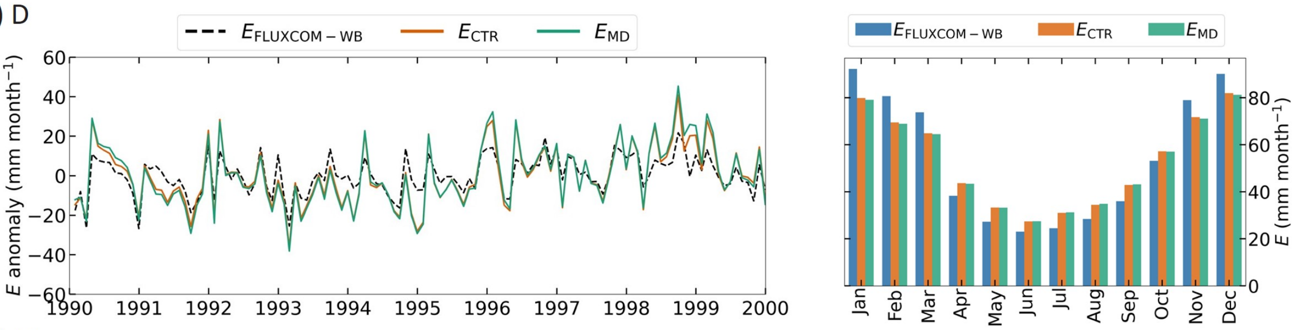

(j) Mu

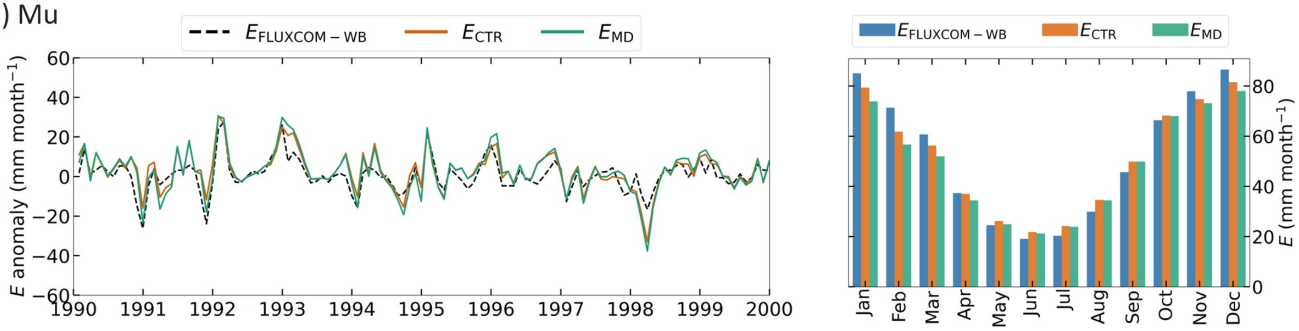

(k) Na

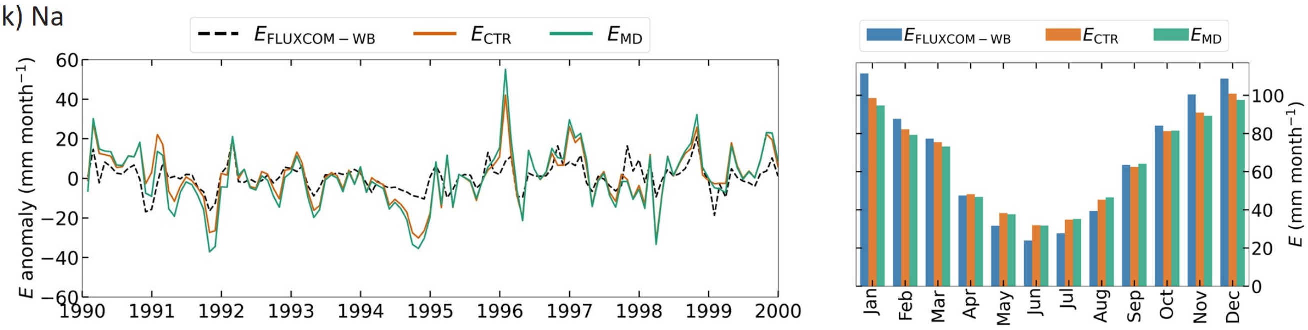

(l) P

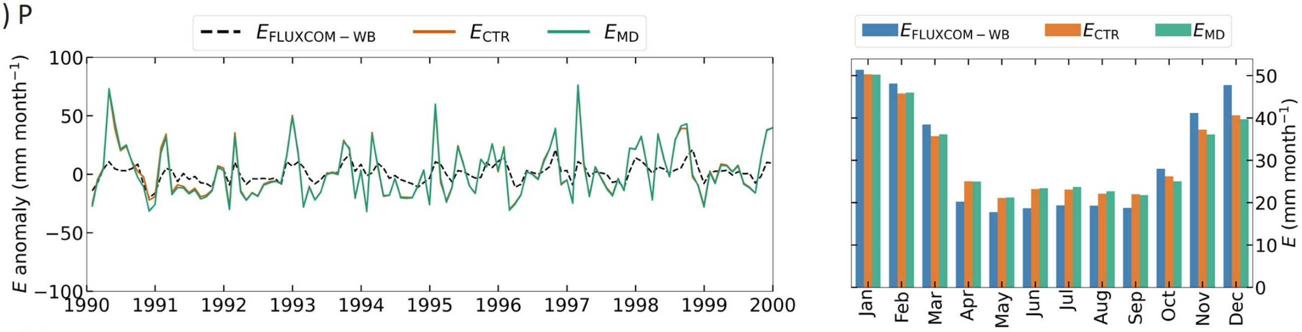

(m) Av

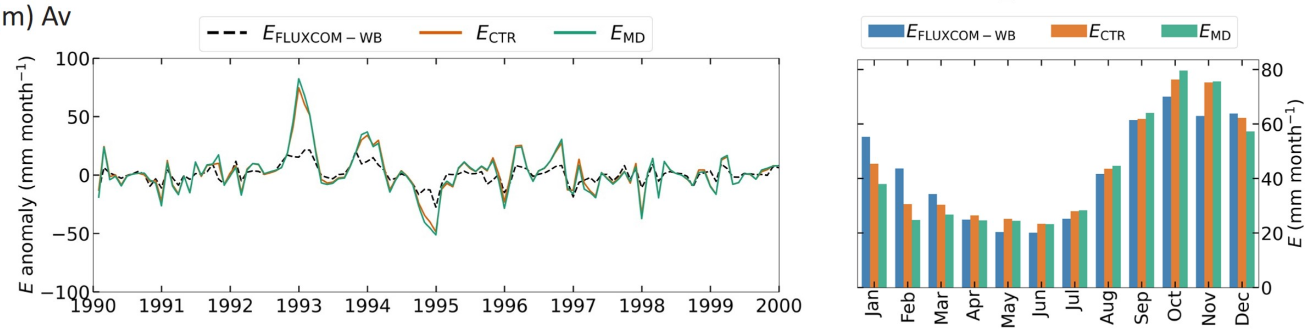

(n) K

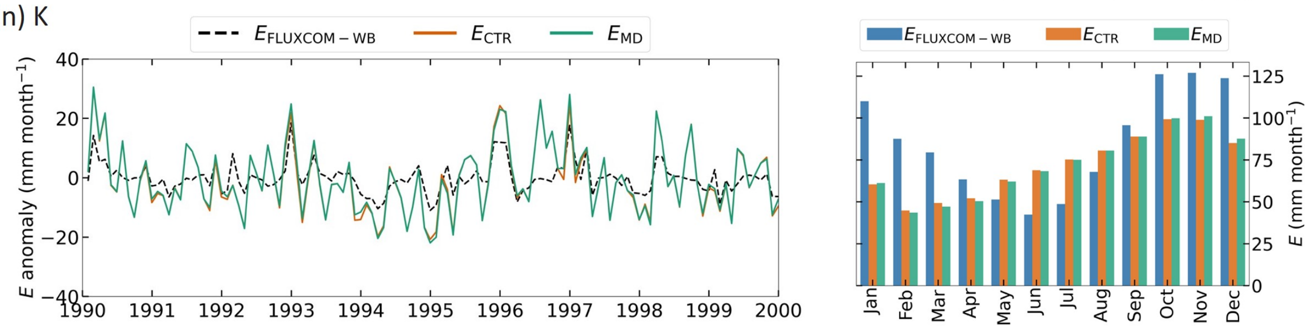

(o) R

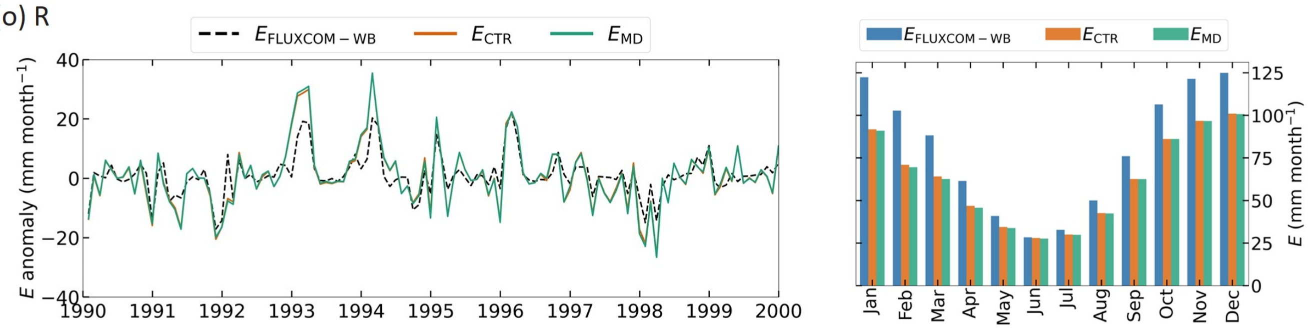

S3.5 Effective root zone storage capacity

Figure S3 presents an analysis of the model S_r computed using the modelled soil moisture deficits and an extreme value analysis as done in the memory method ($S_\mathrm{r,eff}$). From this figure it is confirmed that the $S_\mathrm{r,CTR}$ estimates implied by the model soil depth are larger than the effectively used S_r in CTR ($S_\mathrm{r,CTR,eff}$) (Fig. S3c). This is likely related to the relatively small root percentage in layer 4 prescribed from look-up tables in this layer for most vegetation types compared to the other layers. In contrast with the finding that $S_\mathrm{r,CTR}$ is larger than $S_\mathrm{r,MM}$ in most catchments (Fig. S3a), the $S_\mathrm{r,CTR,eff}$ is smaller than $S_\mathrm{r,MM}$ in 5 tropical and 2 Mediterranean catchments (Fig. S3b). On the other hand, the $S_\mathrm{r,MM}$ we implemented in the MD model is in general close to $S_\mathrm{r,MD,eff}$ being based on modelled soil moisture deficits in the MD model, with slightly larger deviations in the aforementioned 5 tropical and 2 Mediterranean catchments (Fig S3d). In follow-up studies on the model S_r we need to further investigate the role of the root distribution parameter that is likely causing the apparent deviations between the soil depth based S_r and $S_\mathrm{r,eff}$.

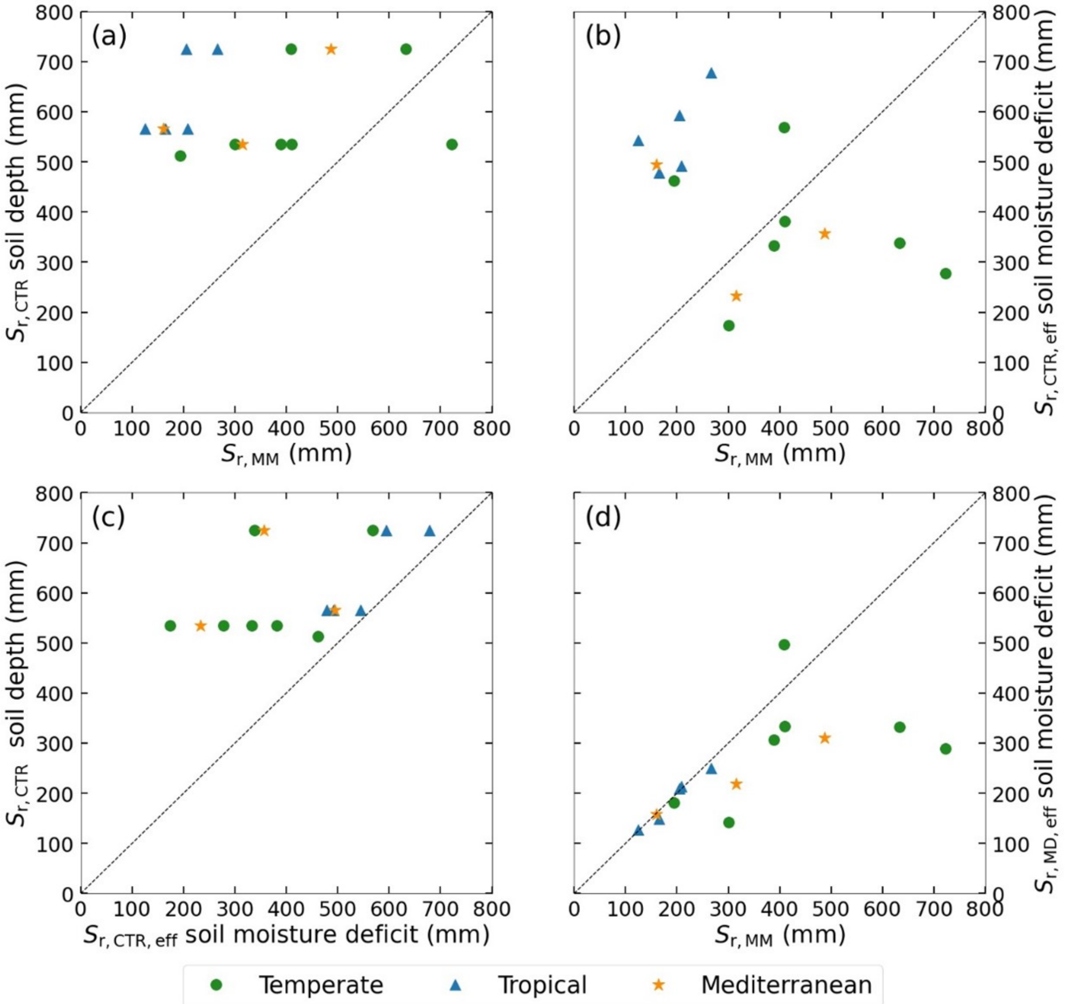

Figure S3.3: Model S_r analysis. (a) $S_\mathrm{r,MM}$ from the memory method vs. $S_\mathrm{r,CTR}$ based on HTESSEL soil depth. (b) $S_\mathrm{r,MM}$ from the memory method vs. $S_\mathrm{r,CTR,eff}$ based on modelled soil moisture deficits. (c) $S_\mathrm{r,CTR}$ based on soil depth vs. $S_\mathrm{r,CTR,eff}$ based on modelled soil moisture deficits. (d) $S_\mathrm{r,MM}$ from the memory method vs. $S_\mathrm{r,MD,eff}$ based on modelled soil moisture deficits

S3.6 Data and code availability

The scripts underlying this chapter are available on https://github.com/fvanoorschot/Python-scripts-van-Oorschot-2021/ or https://zenodo.org/doi/10.5281/zenodo.11198776. Data underlying this chapter is available on https://zenodo.org/doi/10.5281/zenodo.11198819

Supporting information for chapter 4: Influence of irrigation on root zone storage capacity estimation

S4.1 Catchment stratification

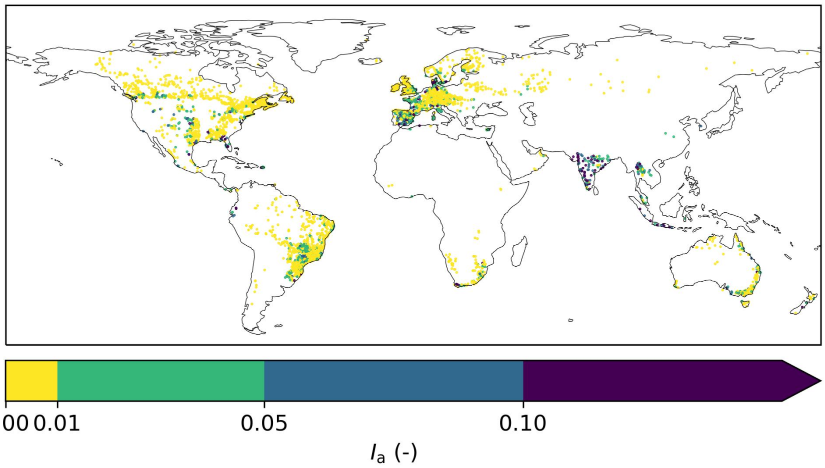

Figure S4.1: Irrigated area fraction (I_{a}) stratified in the four groups used in Fig. 4.7 with dots representing the catchment outlets.

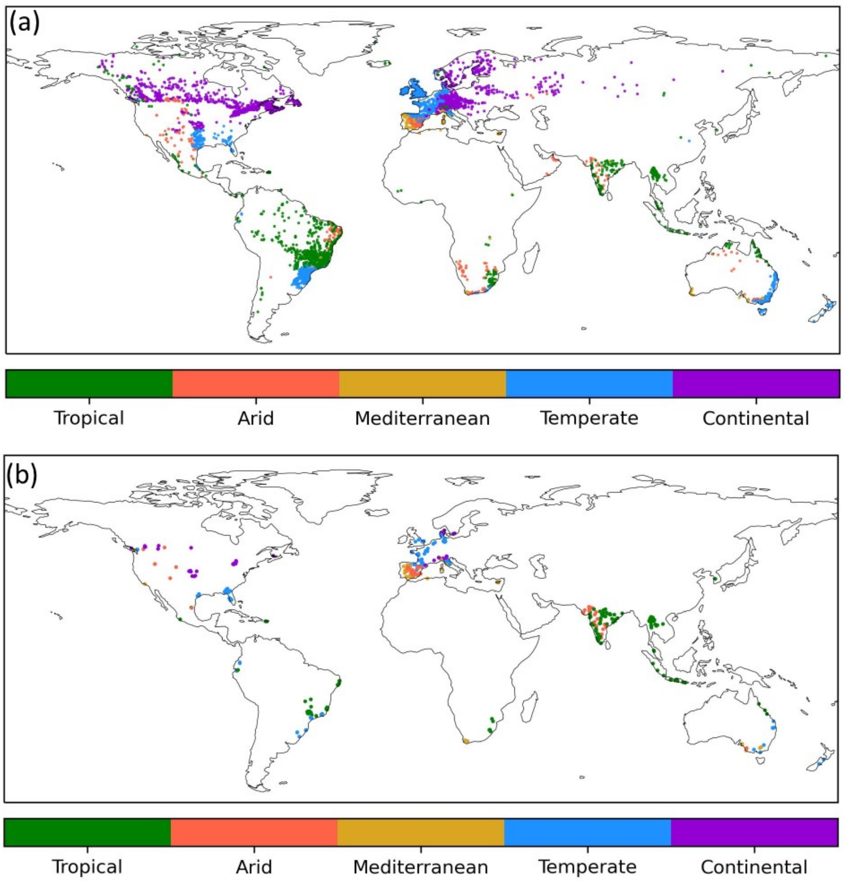

Figure S4.2: Climate zone stratification used in Fig. 4.8b. (a) shows all study catchments and (b) catchments with I_{a}¿0.05. The following classification based on Koppen-Geiger is used: tropical (Af, Am, Aw), arid (BWh, BWk, BSh, BSk), temperate dry summer (Cfa, Cfb, Cfc), Mediterranean(Csa, CSb), and continental (Dfa, Dfb, Dfc, Dfd).

S4.2 Additional results

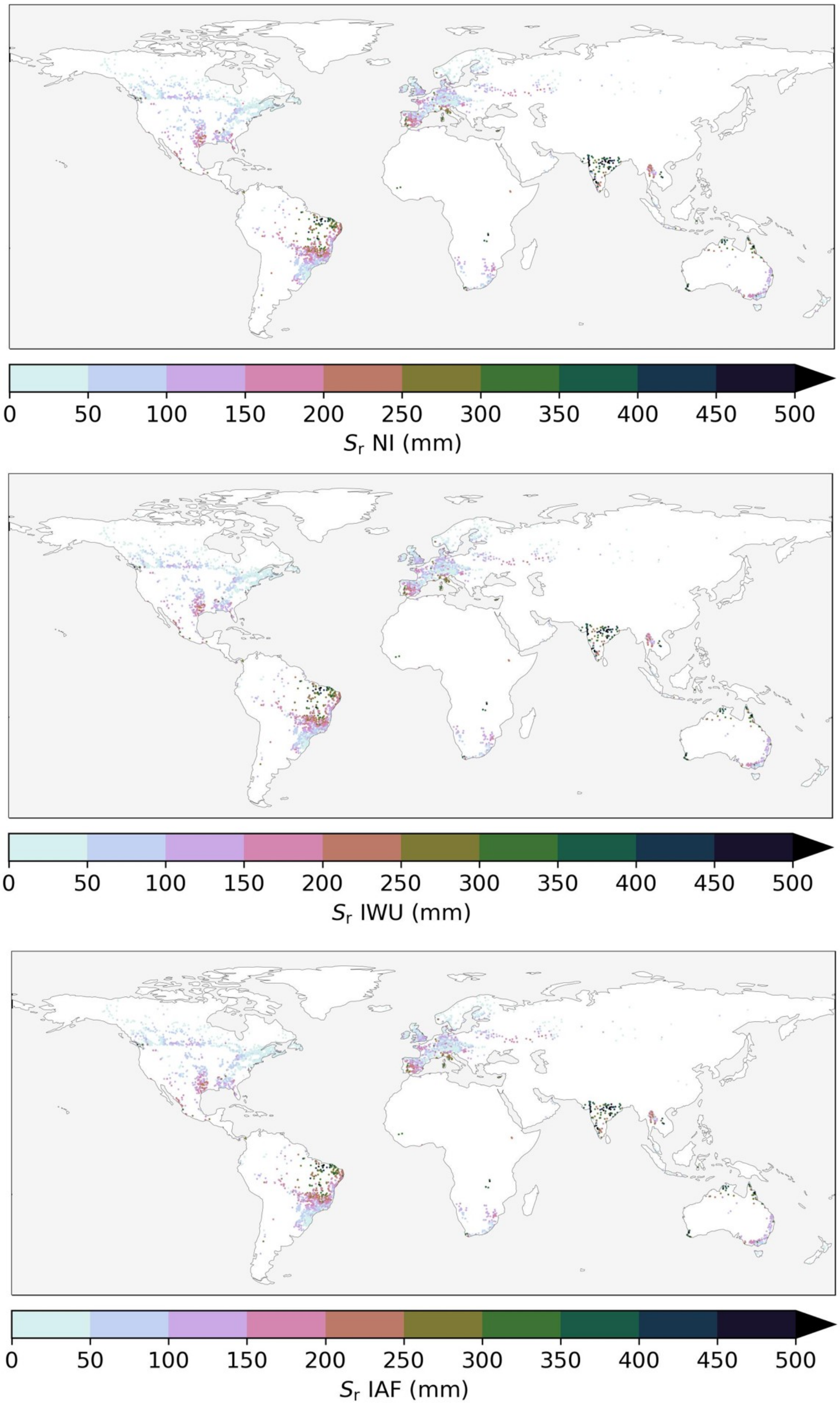

Figure S4.3: Catchment S_r in mm for (a) the No Irrigation (NI) case, (b) the IWU irrigation case, and (c) the IAF irrigation case (Table 4.1), with dots representing catchment outlets.

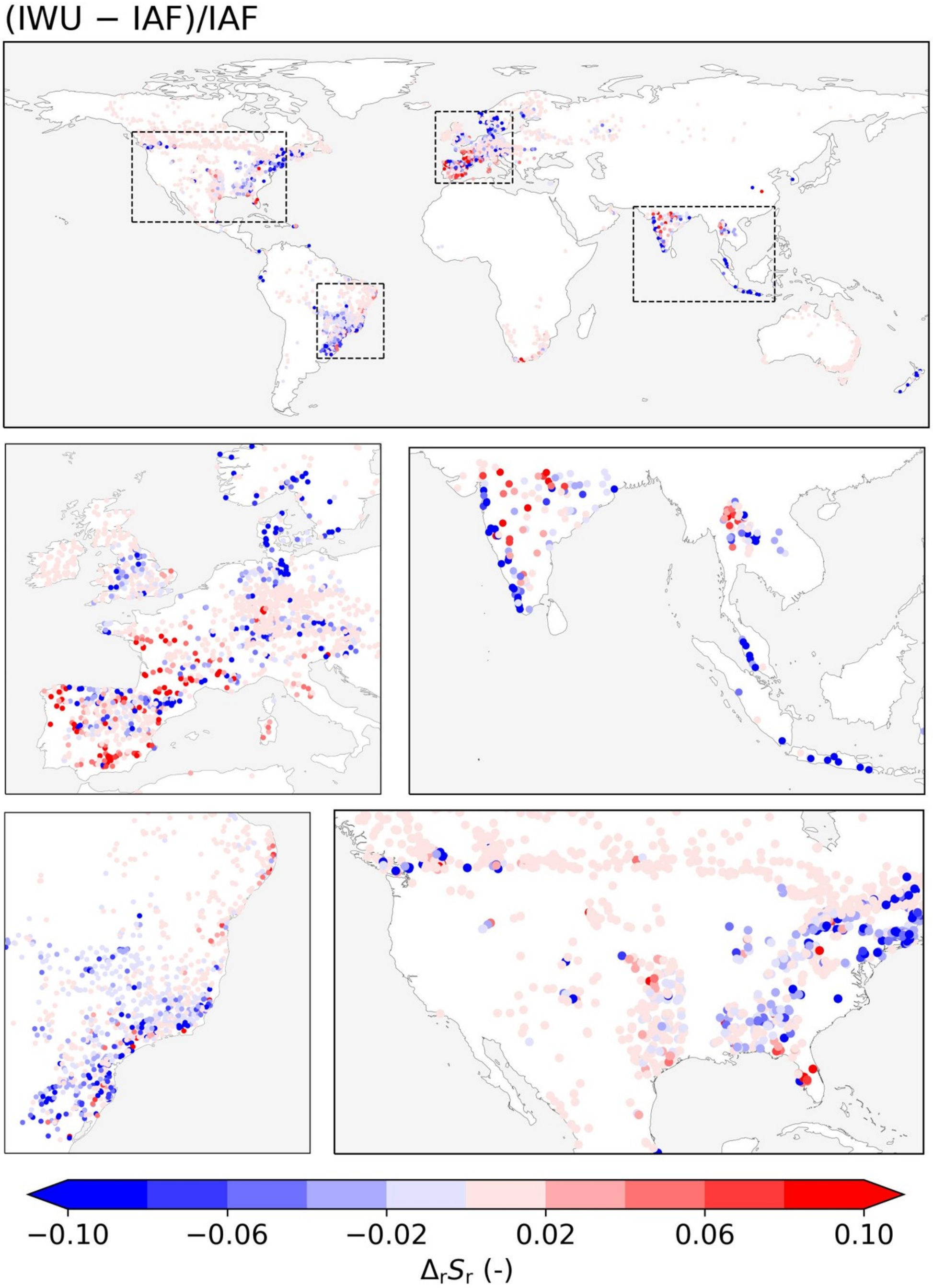

Figure S4.4: Relative difference in S_r ($\Delta_r S_r$ (-)) for IWU compared to IAF ((IWU-IAF)/IAF). See Table 4.1 for details on the irrigation cases.

S4.3 Data and code availability

The scripts underlying this chapter are available on https://github.com/fvanoorschot/python_scripts_vanoorschot2024 or https://doi.org/10.5281/zenodo.11026863. Data underlying this chapter is available on https://doi.org/10.5281/zenodo.10869653.

Supporting information for chapter 5: The global variability in root zone storage capacity explained

S5.1 Random forest model details

For the random forest model, we used the RandomForestRegressor module from the scikit-learn (version 1.0.1) Python package (Pedregosa et al., 2011). We applied a grid search to tune the model hyperparameters namely the maximum number of trees (n_t), the maximum depth of a single tree (d_{max}), and the minimum number of samples required to create a leaf (l_{min}). In this grid search we tested the following parameter values: n_t: 100, 200 and 400 d_{max}: 5, 10 and undefined l_{min}: 1, 5 and 10 All the other hyperparameters are set to the initial values, as explained in the RandomForestRegressor documentation: (https://scikit-learn.org/stable/modules/generated/sklearn.ensemble.RandomForestRegressor.html) Table S1 provides the results of the hyperparameter tuning for the nested cross validation with 5 outer and 5 inner folds (Sect. 5.2.3). The table shows the three best (lowest test MAD) configurations, represented by the rank, for each of the five outer cross validation (CV) folds. Based on these results, we concluded that $l_{min} = 1$, and d_{max}=undefined provide the lowest test MAD in all cases. The differences between the test MAD for the different values of n_t are relatively small. Therefore, we selected the simplest option with $n_t = 100$.

Table S5.1: Hyperparameter tuning results for the nested cross validation with 5 outer and 5 inner folds (Sect. 5.2.3). A grid search has been done to find the best model parameters for the number of trees (n_t) of 100, 200, and 400; the maximum depth of a single tree (d_{max}) of 5, 10 or undefined; and the minimum number of samples required to create a leaf (l_{min}) of 1, 5, and 10. The table shows the three best (lowest test MAD) configurations for each of the five outer cross validation (CV) folds.

CV fold	Rank	$\mathbf{n_t}$	$\mathbf{d_{max}}$	$\mathbf{l_{min}}$	Train MAD	Test MAD	n train	n test
1	1	400	Undefined	1	13.6	36.7	2555	639
1	2	200	Undefined	1	13.7	36.8	2555	639
1	3	100	Undefined	1	13.9	36.9	2555	639
2	1	400	Undefined	1	13.7	37.2	2555	639
2	2	200	Undefined	1	13.8	37.2	2555	639
2	3	100	Undefined	1	13.9	37.6	2555	639
3	1	400	Undefined	1	13.9	37.1	2555	639
3	2	200	Undefined	1	14.0	37.3	2555	639
3	3	100	Undefined	1	14.0	37.4	2555	639
4	1	400	Undefined	1	13.8	37.0	2555	639
4	2	200	Undefined	1	13.8	37.1	2555	639
4	3	100	Undefined	1	13.9	37.2	2555	639
5	1	400	Undefined	1	14.0	36.5	2556	638
5	2	200	Undefined	1	14.0	36.8	2556	638
5	3	100	Undefined	1	14.1	36.8	2556	638

S5.2 Cross correlation tables

	$\overline{P}$	$\overline{E}_p$	$\overline{T}$	T_d	$\overline{t_{IS}}$	I_{S,E_p}	$I_{S,P}$	I_{AS}	d_b	I_a	s	e	f_{tree}	$f_{nontree}$	f_{nonveg}	f_{clay}	f_{sand}	$\overline{LAI}$	v_{LAI}	$\overline{f}_{snow}$	$f_{snow,v}$
$\overline{P}$		.49	.37	-.47	-.25	-.54	.06	-.07	-.02	-.03	.13	-.20	.39	-.12	-.49	.29	-.10	.59	-.26	-.20	-.27
$\overline{E}_p$	.49		.86	-.66	.22	-.91	.48	-.25	.18	.09	-.11	-.05	.05	.17	-.32	.61	-.01	.40	-.50	-.64	-.52
$\overline{T}$	.37	.86		-.77	.32	-.87	.51	-.20	.27	.19	-.31	-.20	-.26	.47	-.23	.72	-.14	.20	-.45	-.83	-.47
T_d	-.47	-.66	-.77		-.19	.81	-.49	-.04	-.12	-.13	-.09	-.07	.15	-.34	.24	-.58	-.00	-.26	.63	.58	.51
$\overline{t_{IS}}$	-.25	.22	.32	-.19		-.22	.59	.17	.28	.16	-.05	.16	-.43	.19	.45	.17	.09	-.34	-.15	-.23	-.20
I_{S,E_p}	-.54	-.91	-.87	.81	-.22		-.48	.20	-.17	-.11	.02	.01	-.02	-.21	.33	-.60	.04	-.40	.50	.67	.47
$I_{S,P}$	.06	.48	.51	-.49	.59	-.48		.05	.40	.16	.01	.21	-.38	.38	.10	.40	.13	-.20	-.28	-.24	-.49
I_{AS}	-.07	-.25	-.20	-.04	.17	.20	.05		-.09	.10	.20	-.02	-.08	-.06	.22	-.30	.16	-.15	-.14	.17	.14
d_b	-.02	.18	.27	-.12	.28	-.17	.40	-.09		.26	-.21	-.03	-.29	.27	.12	.21	-.09	-.16	.11	-.18	-.12
I_a	-.03	.09	.19	-.13	.16	-.11	.16	.10	.26		-.08	-.06	-.20	.19	.06	.11	-.01	-.11	-.05	-.20	-.03
s	.13	-.11	-.31	-.09	-.05	.02	.01	.20	-.21	-.08		.64	.18	-.31	.14	-.23	.15	.03	-.20	.46	-.09
e	-.20	-.05	-.20	-.07	.16	.01	.21	-.02	-.03	-.06	.64		-.16	-.08	.39	-.05	.12	-.28	-.24	.34	-.16
f_{tree}	.39	.05	-.26	.15	-.43	-.02	-.38	-.08	-.29	-.20	.18	-.16		-.81	-.54	-.29	.17	.67	.04	.29	.05
$f_{nontree}$	-.12	.17	.47	-.34	.19	-.21	.38	-.06	.27	.19	-.31	-.08	-.81		-.06	.52	-.25	-.38	-.10	-.48	-.21
f_{nonveg}	-.49	-.32	-.23	.24	.45	.33	.10	.22	.12	.06	.14	.39	-.54	-.06		-.25	.07	-.59	.07	.20	.21
f_{clay}	.29	.61	.72	-.58	.17	-.60	.40	-.30	.21	.11	-.23	-.05	-.29	.52	-.25		-.57	.12	-.33	-.67	-.40
f_{sand}	-.10	-.01	-.14	-.00	.09	.04	.13	.16	-.09	-.01	.15	.12	.17	-.25	.07	-.57		-.07	-.16	.33	-.20
$\overline{LAI}$	.59	.40	.20	-.26	-.34	-.40	-.20	-.15	-.16	-.11	.03	-.28	.67	-.38	-.59	.12	-.07		-.22	-.20	-.07
v_{LAI}	-.26	-.50	-.45	.63	-.15	.50	-.28	-.14	.11	-.05	-.20	-.24	.04	-.10	.07	-.33	-.16	-.22		.27	.43
$\overline{f}_{snow}$	-.20	-.64	-.83	.58	-.23	.67	-.24	.17	-.18	-.20	.46	.34	.29	-.48	.20	-.67	.33	-.20	.27		.10
$f_{snow,v}$	-.27	-.52	-.47	.51	-.20	.47	-.49	.14	-.12	-.03	-.09	-.16	.05	-.21	.21	-.40	-.20	-.07	.43	.10	

Figure S5.1: Correlation matrix for the 21 catchment descriptors described in Table 5.1. Values indicate the Pearson correlation coefficient and blue (red) colors represent the strength of the positive (negative) correlation.

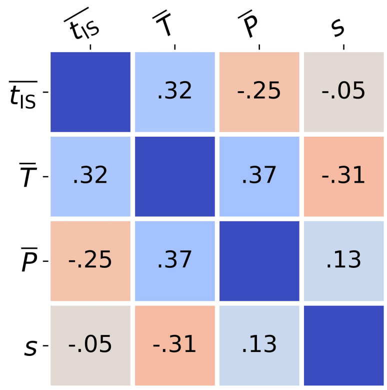

Figure S5.2: Correlation matrix for the 4 catchment descriptors described in Table 5.1. Values indicate the Pearson correlation coefficient and blue (red) colors represent the strength of the positive (negative) correlation.

S5.3 Model results

Table S5.2: Cross validation results for the 21-variable model using a fivefold cross validation. n indicates the number of catchments used for training or testing, and the MAD is the mean absolute difference between the predicted and the memory method root zone storage capacity.

Cross-validation fold	**n train**	**n test**	**MAD train (mm)**	**MAD test (mm)**
1	2889	723	13	34
2	2889	723	13	37
3	2890	722	13	36
4	2890	722	13	36
5	2890	722	13	33

Table S5.3: Same as Table S5.2 for the 4-variable model.

Cross-validation fold	**n train**	**n test**	**MAD train (mm)**	**MAD test (mm)**
1	2889	723	15	38
2	2889	723	14	41
3	2890	722	15	39
4	2890	722	15	39
5	2890	722	15	37

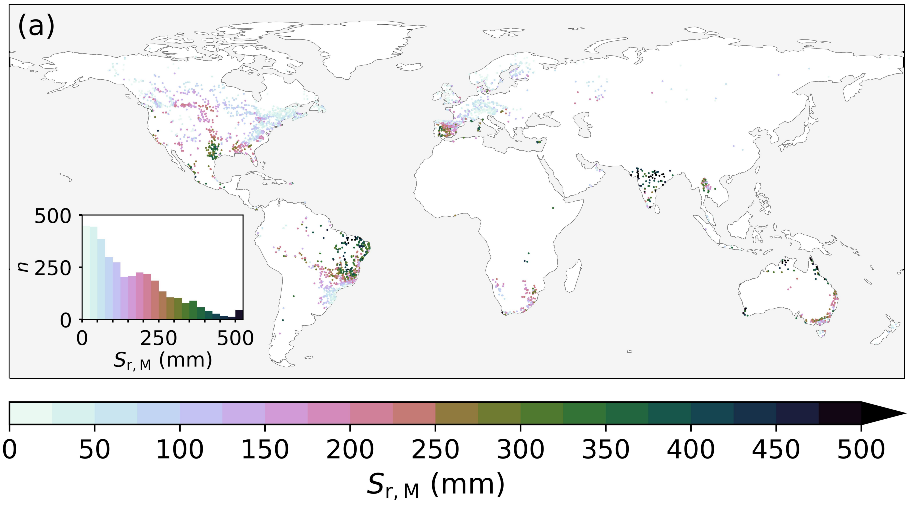

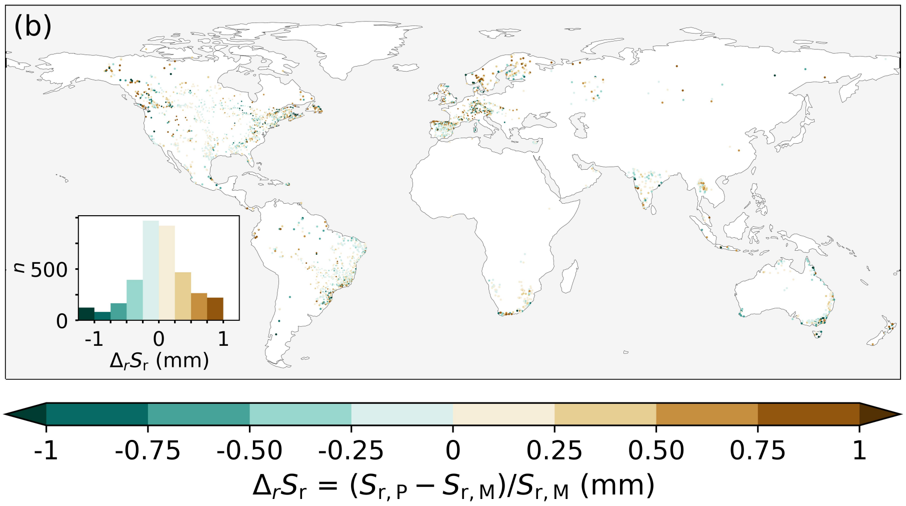

Figure S5.3: (a) Memory method root zone storage capacity ($S_{\mathrm{r,M}}$ (mm)). (b) Relative difference between the 4-variable model predicted and memory method: $\Delta_{\mathrm{rel}} S_{\mathrm{r}} = (S_{\mathrm{r,P}} - S_{\mathrm{r,M}})/S_{\mathrm{r,M}}$ of the evaluation data of all fivefold cross validation models combined.

S5.4 Global comparison of root characteristics

Table S5.4: Details of the global datasets of root characteristics used in Fig. 5.7.

Reference	Variable	Method description	Data reference
Wang-Erlandsson (2016)	Root zone storage capacity	Based on cumulative water deficits, including irrigation. Gumbel-normalized with a 20 years return period	http://dx.doi.org/10.5194/hess-20-1459-2016-supplement
Stocker et al. (2023)	Root zone storage capacity	Based on cumulative water deficits. Gumbel-normalised with a 80 year return period	https://doi.org/10.5281/zenodo.5515246
Kleidon et al. (2004)	Optimised hydrologically active rooting depth	Estimated by optimised inverse modelling. Hydrologically active rooting depth is based on a maximization of net primary production.	Upon request to the author
Fan et al. (2017)	Maximum depth of root water uptake	Inverse model based on (1) soil water supply based on hydrological model using observed climate, soil properties and topography; (2) ecosystem water demand from LAI and reanalysis atmosphere; (3) given (1) and (2) estimate necessary depths of water uptake to meet the demand	https://wci.earth2observe.eu/thredds/catalog/usc/root-depth/catalog.html
Yang et al. (2016)	Effective plant rooting depth	Balance of carbon cost and benefit of root development (Guswa et al., 2008); an optimal rooting depth at which the marginal carbon benefit associated with any additional roots balances the marginal carbon cost of those roots	http://doi.org/10.4225/08/5837b3aa9cb90
Schenk et al. (2009)	95% rooting depth	Estimated rooting depths for 95% of the roots based on observed rooting depths (Schenk and Jackson, 2003)	https://daac.ornl.gov/cgi-bin/dsviewer.pl?ds_id=929
Schenk and Jackson (2003)	Extrapolated 95% rooting depths	Estimated from a global database of root profiles assembled from the primary literature to study relationships of abiotic and biotic factors associated with belowground vegetation structure.	https://daac.ornl.gov/cgi-bin/dsviewer.pl?ds_id=660

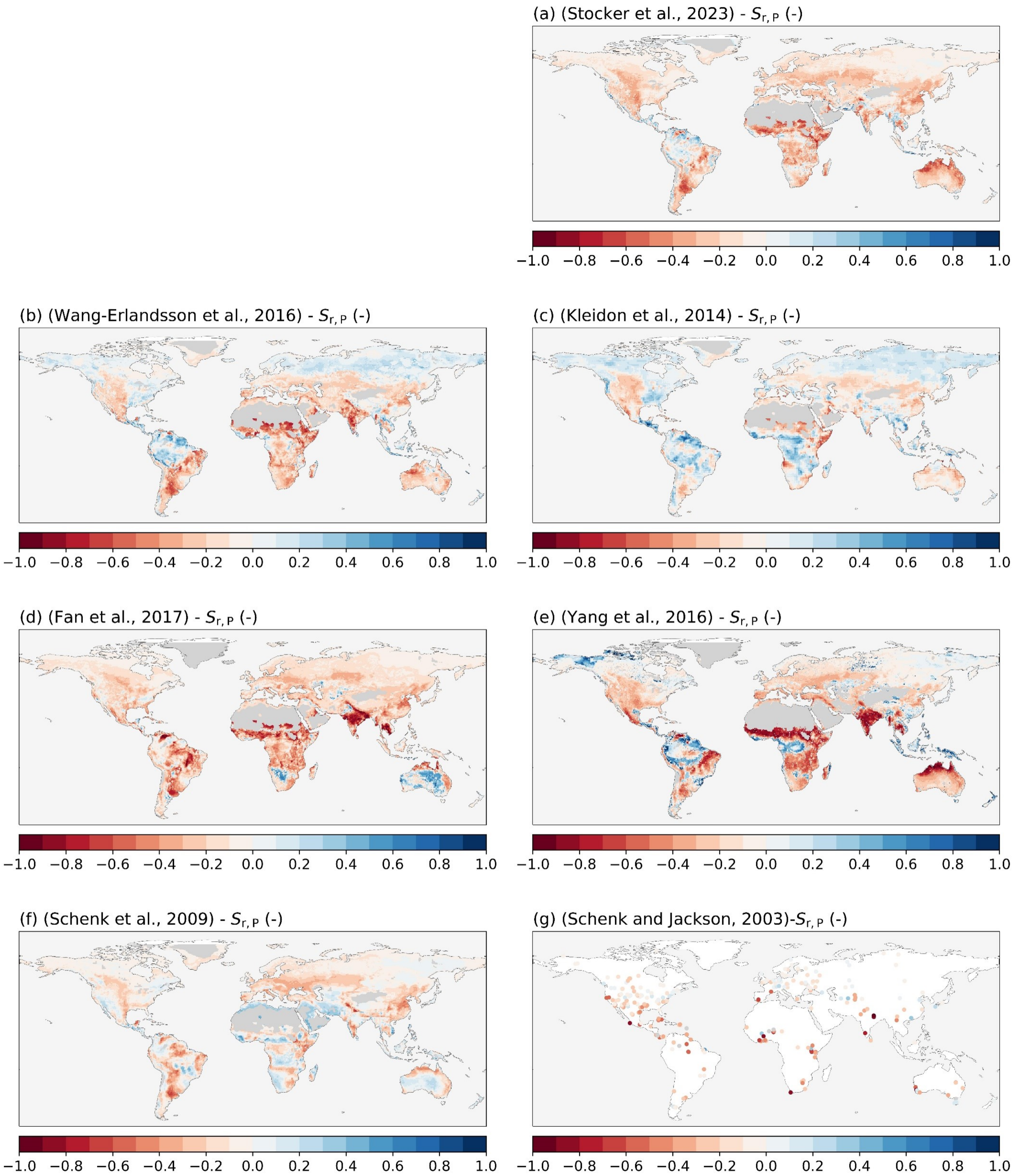

Figure S5.4: Difference maps between normalized vegetation root characteristics presented in Fig. 5.7.

S5.5 Data and code availability

The scripts underlying this chapter are available on https://github.com/fvanoorschot/python_scripts_global_sr_controls or https://zenodo.org/doi/10.5281/zenodo.11260711. Data underlying this chapter is available on https://zenodo.org/doi/10.5281/zenodo.11259390.

Supporting information for chapter 6: Conclusions

S6.1 Data and code availability

The scripts underlying this chapter are available on https://github.com/fvanoorschot/python_scripts_chapter6 or https://doi.org/10.5281/zenodo.11235083. Data underlying this chapter is available on https://zenodo.org/doi/10.5281/zenodo.11235097.